

Contents lists available at ScienceDirect

### **Computers and Mathematics with Applications**

journal homepage: www.elsevier.com/locate/camwa



## Linear second order energy stable schemes for phase field crystal growth models with nonlocal constraints



Xiaobo Jing<sup>a</sup>, Oi Wang<sup>b,a,\*</sup>

- <sup>a</sup> Beijing Computational Science Research Center, Beijing 100193, PR China
- <sup>b</sup> Department of Mathematics, University of South Carolina, Columbia, SC 29028, USA

#### ARTICLE INFO

# Article history: Received 10 December 2018 Received in revised form 24 June 2019 Accepted 26 July 2019 Available online 1 October 2019

Keywords:
Allen-Cahn equation with nonlocal constraints
Phase field model
Crystal growth
Energy stable schemes
Energy quadratization

#### ABSTRACT

We present a set of linear, second order, unconditionally energy stable schemes for the Allen–Cahn model with nonlocal constraints for crystal growth that conserves the mass of each phase. Solvability conditions are established for the linear systems resulting from the schemes. Convergence rates are verified numerically. Dynamics obtained using the Allen–Cahn model with nonlocal constraints are compared with the one obtained using the classic Allen–Cahn model as well as the Cahn–Hilliard model, respectively, demonstrating slower dynamics than that of the Allen–Cahn model but faster dynamics than that of the Cahn–Hilliard model. Thus, the Allen–Cahn model with nonlocal constraints can serve as an alternative to the Cahn–Hilliard model in simulating crystal growth while conserving the mass of each phase. Two Benchmark examples are presented to contrast the predictions made with the four models, highlighting the accuracy and effectiveness of the Allen–Cahn model with nonlocal constraints.

© 2019 Published by Elsevier Ltd.

#### 1. Introduction

Phase field crystal (PFC) growth model, developed as an extension to the phase field formalism [1–5], has been successfully applied to various applications in materials science across different time scales [6–8], capturing the interaction between material defects [1] and modeling the microstructure evolution [1,2,6,9–15]. It is a challenge to develop efficient and stable numerical algorithms to faithfully simulate dynamics described by PFC models. The PFC model is thermodynamically consistent in that the free energy of the thermodynamic model is dissipative. Numerical algorithms that respect the free energy dissipation property at the discrete level are known as energy stable schemes.

The Cahn-Hilliard equation is a popular phase field model for crystal growth because of its mass (or volume) preserving property. However, the Cahn-Hilliard equation for the crystal growth problem is of up to the 6th order spatial derivative. For most crystal growth models, transient dynamics is less important than the correct crystal growth pattern that the model yields, which is dominated by the free energy of the model. Searching for a lower order phase field model that can also preserve mass and free energy dissipation properties is therefore a viable alternative. Allen-Cahn equation is a popular phase field model which normally has lower spatial derivatives than the Cahn-Hilliard model. It describes relaxation dynamics of the thermodynamical system to equilibrium. However, in the case of a phase field description, when the phase variable represents the mass density, fraction or the volume fraction of a material component, this model does not warrant the conservation of mass or volume of that component. In order to conserve mass, the free energy functional has to be augmented by a mass preserving penalty term or with a Lagrange multiplier [16–20]. This henceforth modifies the

<sup>\*</sup> Corresponding author at: Department of Mathematics, University of South Carolina, Columbia, SC 29028, USA. E-mail address: qwang@math.sc.edu (Q. Wang).

Allen–Cahn equation into a nonlocal equation. We call this the nonlocal Allen–Cahn model or the Allen–Cahn model with nonlocal constraints.

Rubinstein and Sternberg studied the Allen–Cahn model with a mass constraint analytically and compared it to the Cahn–Hilliard model [18]. Their result seems to favor using the Allen–Cahn model with a mass constraint in place of the Cahn–Hilliard model when studying interfacial dynamics of incompressible, immiscible multi-component material systems.

For the classical Allen–Cahn equation as well as the Cahn–Hilliard equation, there have been several popular numerical approaches to construct energy stable schemes for the equations, including the convex splitting approach [21–27], the stabilizing approach [28–30], the energy quadratization (EQ) approach [31–34] and the scalar auxiliary variable approach [35–37]. Recently, the energy quadratization (EQ) and its reincarnation in the scalar auxiliary variable (SAV) method have been applied to a host of thermodynamic and hydrodynamic models owing to their simplicity, ease of implementation, computational efficiency, linearity, and most importantly their energy stability property [32–34,36–46]. It has been shown that these strategies are general enough to be useful for developing energy stable numerical approximations to any thermodynamically consistent models, i.e., the models satisfy the second law of thermodynamics or are derived from the Onsager principle [31,47,48]. The convex splitting, stabilizing, scalar auxiliary variable, energy quadratization approach and other methods have been applied to the Cahn–Hilliard model for crystal growth [24,31,49–57].

In this paper, we develop a set of linear, second order, unconditionally energy stable schemes using the energy quadratization (EQ) and scalar auxiliary variable (SAV) approach to solve the Allen–Cahn equation with nonlocal constraints numerically. The numerical schemes for the Allen–Cahn and the Cahn–Hilliard model are recalled in the paper simply for introducing the nonlocal Allen–Cahn models and comparison purposes. In some of these schemes, both EQ and SAV methods are combined to yield linear, energy stable schemes. We note that when a nonlocal Allen–Cahn model is discretized, it is inevitable to yield an integral term which can be effectively treated with a scalar auxiliary variable. When multiple integrals are identified as SAVs in the free energy functional of the Allen–Cahn model with nonlocal constraints, new solution procedures are developed to solve the subproblems in which elliptic equations can be solved efficiently. All these schemes are linear and second order accurate in time. On the other hand, when the EQ strategy is coupled with the discretized integrals, the Sherman–Morrison formula can lead us to an efficient numerical scheme as well. In fact, this can be equivalently dealt with using the SAV method, which will be discussed in the Appendix. The numerical schemes developed in this study for the Allen–Cahn equation with nonlocal constraints preserve not only mass but also the energy dissipation rate at the discrete level.

In the end, we conduct some numerical experiments to assess the performance of the schemes as well as the comparison between dynamics of the nonlocal Allen–Cahn models and that of the Cahn–Hilliard. The results based on EQ and those based on SAV methods perform equally well in preserving mass and the energy dissipation rate. In addition, the computational efficiency of the schemes is comparatively studied in one of the benchmark examples as well. To simplify the presentation, we present the temporal discretization of the models using EQ and SAV approaches in detail. Then, we only briefly discuss the strategy to obtain fully discrete schemes by discretizing the semi-discrete schemes in space. We refer readers to our early publications in [33,34] for details. We show that the linear systems resulting from the schemes are all solvable uniquely if the time step size is suitable so that the solution existence and uniqueness in the full-discrete system is warranted. With the free energy density for crystal growth, the Allen–Cahn model with nonlocal constraints compares well with the Cahn–Hilliard model in yielding transient dynamics and steady state crystalline patterns. The numerical schemes for the Allen–Cahn model with nonlocal constraints consistently perform better than those for the Cahn–Hilliard model at larger time steps.

The rest of the paper is organized as follows. In Section 2, we present the mathematical models for the classical Allen–Cahn, the Cahn–Hilliard, and the Allen–Cahn model with nonlocal constraints. In Section 3, we compare their near equilibrium dynamics. In Section 4, we present a set of second order, linear, energy stable numerical schemes for the models. In Section 5, we conduct mesh refinement tests on all the schemes and carry out two simulations on crystal growth as well as its grain-boundary effects using the models. Finally, we give the concluding remark in Section 6.

#### 2. Phase field models for crystal growth

We consider a phase field model for modeling crystal growth in solids with a focus on resolving the detail of transient dynamics. The free energy of the phase field model for crystal growth is given by [2,4,54]

$$F = \int_{\Omega} \left[ \frac{\phi}{2} (-\varepsilon + (\nabla^2 + 1)^2) \phi + \frac{\phi^4}{4} \right] d\mathbf{r}, \tag{2.1}$$

where  $\phi$  represents an atomistic density field, which is the deviation of the density from the average density and is a conserved field variable,  $\epsilon$  is a parameter related to the temperature, that is, higher  $\epsilon$  corresponds to a lower temperature, and  $\nabla$  is the gradient operator ( $\nabla^2$  denotes the Laplacian). In this study, we use a more general form of the free energy

given by

$$F = \int_{\Omega} \left[ \frac{\phi}{2} (\nabla^4 + 2a\nabla^2 + \alpha)\phi + \frac{\phi^4}{4} \right] d\mathbf{r}$$

$$= \int_{\Omega} \left[ \frac{1}{2} (\|\nabla^2 \phi\| + a\phi)^2 + \frac{\alpha - a^2}{2} \phi^2 + \frac{\phi^4}{4} \right] d\mathbf{r}$$

$$= \int_{\Omega} \left[ \frac{1}{2} \|\nabla^2 \phi\|^2 - a\|\nabla \phi\|^2 + \frac{\alpha}{2} \phi^2 + \frac{\phi^4}{4} \right] d\mathbf{r},$$
(2.2)

where  $a=1, \alpha=1-\varepsilon$  recovers Eq. (2.1). In the above derivation, the following the boundary conditions are assumed

$$\mathbf{n} \cdot \nabla \phi = 0, \quad \mathbf{n} \cdot \nabla \nabla^2 \phi = 0. \tag{2.3}$$

Based on the Onsager linear response theory [47,48], transient dynamics of such a system is customarily governed by a time-dependent partial differential equation given by

$$\frac{\partial \phi}{\partial t} = -M\mu, \quad \mathbf{rin} \, \Omega, \, t > 0, 
\mu = \frac{\delta F}{\delta \phi} = (\nabla^2 + a)^2 \phi + (\alpha - a^2) \phi + \phi^3,$$
(2.4)

subject to appropriate boundary and initial conditions, where M and  $\mu = \frac{\delta F}{\delta \phi}$  are the mobility matrix and the chemical potential, respectively.

The time rate of change of the free energy is given by

$$\frac{dF}{dt} = -\int_{\Omega} \mu M \mu d\mathbf{r} + \int_{\partial\Omega} \mathbf{n} \cdot \left[ \left( \frac{\partial f}{\partial \nabla \phi} - \nabla \frac{\partial f}{\partial \nabla^2 \phi} \right) \phi_t + \frac{\partial f}{\partial \nabla^2 \phi} \nabla \phi_t \right] d\mathbf{s}. \tag{2.5}$$

The following boundary conditions will annihilate the boundary terms in the energy dissipation functional

$$\mathbf{n} \cdot \nabla \phi = 0, \quad \mathbf{n} \cdot (\frac{\partial f}{\partial \nabla \phi} - \nabla \frac{\partial f}{\partial \nabla^2 \phi}) = 0. \tag{2.6}$$

In the crystal growth model,  $\frac{\partial f}{\partial \nabla \phi}=0$ . So, the boundary conditions reduce to

$$\mathbf{n} \cdot \nabla \phi = 0, \quad \mathbf{n} \cdot \nabla \frac{\partial f}{\partial \nabla^2 \phi} = \mathbf{n} \cdot \nabla \nabla^2 \phi = 0,$$
 (2.7)

which is boundary conditions given in (2.3).

An alternative set of boundary conditions that annihilate the boundary contribution to energy dissipation is given by

$$\frac{\partial f}{\partial \nabla^2 \phi} = 0, \quad \mathbf{n} \cdot (\frac{\partial f}{\partial \nabla \phi} - \nabla \frac{\partial f}{\partial \nabla^2 \phi}) = 0. \tag{2.8}$$

This is equivalent to

$$(\nabla^2 + a)\phi = 0, \qquad \mathbf{n} \cdot (\frac{\partial f}{\partial \nabla \phi} - \nabla \frac{\partial f}{\partial \nabla^2 \phi}) = 0. \tag{2.9}$$

This is different from the previous one.

We can also assign dissipative boundary conditions to the model as follows

$$\mathbf{n} \cdot \nabla \phi_t = 0, \quad \phi_t = -\beta \mathbf{n} \cdot (\frac{\partial f}{\partial \nabla \phi} - \nabla \frac{\partial f}{\partial \nabla^2 \phi}), \tag{2.10}$$

where  $\beta > 0$  is inversely proportional to a relaxation time. The boundary contribution to the energy dissipation is then given by

$$-\int_{\partial\Omega}\beta[\mathbf{n}\cdot(\frac{\partial f}{\partial\nabla\phi}-\nabla\frac{\partial f}{\partial\nabla^2\phi})]^2ds. \tag{2.11}$$

The total energy dissipation rate or energy dissipation functional is given by

$$\frac{dF}{dt} = -\int_{\Omega} \mu M \mu d\mathbf{r} - \int_{\partial\Omega} \beta [\mathbf{n} \cdot (\frac{\partial f}{\partial \nabla \phi} - \nabla \frac{\partial f}{\partial \nabla^2 \phi})]^2 ds. \tag{2.12}$$

If  $\beta \to \infty$ , we recover (2.7). In this study, we will focus on the boundary conditions given in (2.3).

Two well-known dynamic models for  $\phi$  are the Allen–Cahn and the Cahn–Hilliard equation, whose mobility is given respectively by

$$M = \begin{cases} M_0, & \text{Allen-Cahn,} \\ -\nabla \cdot M_0 \nabla, & \text{Cahn-Hilliard,} \end{cases}$$
 (2.13)

where  $M_0$  is a prescribed mobility coefficient matrix, which can be a function of  $\phi$ . The Allen–Cahn equation does not conserve the total mass  $\int_{\Omega} \phi d\mathbf{r}$  if  $\phi$  is the mass density while the Cahn–Hilliard equation does. However, these two models predict similar near equilibrium dynamics. On the other hand the Allen–Cahn equation is an equation of lower spatial derivatives, and presumably costs less when solved numerically. Thus, one can impose the mass conservation as a constraint to the Allen–Cahn equation for it to be used to describe dynamics in which the mass is conserved. Next, we will briefly recall several ways to enforce mass conservation to dynamics described by the Allen–Cahn equation.

#### 2.1. Allen-Cahn model

 $\phi|_{t=0} = \phi(0, \mathbf{x}),$ 

The classical Allen-Cahn equation with the non-flux Neumann boundary conditions is given by

$$\frac{\partial \phi}{\partial t} = -M\mu, \quad \text{in } \Omega, 
\frac{\partial \phi}{\partial n} = 0, \quad \frac{\partial \nabla^2 \phi}{\partial n} = 0, \quad \text{in } \partial \Omega, 
(2.14)$$

where M is the mobility coefficient and  $\mu$  is the chemical potential given by

$$\mu = \frac{\delta F}{\delta \phi} = (\nabla^2 + a)^2 \phi + (\alpha - a^2)\phi + \phi^3. \tag{2.15}$$

The energy dissipation rate of the Allen-Cahn equation is given by

$$\frac{dF}{dt} = \int_{\Omega} \frac{\delta F}{\delta \phi} \phi_t d\mathbf{r} = -\int_{\Omega} \mu(M\mu) d\mathbf{r} \le 0, \tag{2.16}$$

provided nonnegative M. The Allen–Cahn model does not conserve the mass if the mass is denoted as  $\int_{\Omega} \phi d\mathbf{r}$ .

#### 2.2. Cahn-Hilliard model

The Cahn-Hilliard equation with the non-flux Neumann boundary condition is given by

$$\frac{\partial \phi}{\partial t} = \nabla \cdot (M \nabla \mu), \quad \text{in } \Omega, 
\frac{\partial \phi}{\partial n} = 0, \quad \frac{\partial \nabla^2 \phi}{\partial n} = 0, \quad \frac{\partial \mu}{\partial n} = 0 \quad \text{in } \partial \Omega, 
\phi|_{t=0} = \phi(0, \mathbf{x}),$$
(2.17)

where M is the mobility coefficient and  $\mu$  is the chemical potential given by (2.15). The energy dissipation rate of the equation is given by

$$\frac{dF}{dt} = \int_{\Omega} \frac{\delta F}{\delta \phi} \phi_t d\mathbf{r} = -\int_{\Omega} \nabla \mu M \nabla \mu d\mathbf{r} \le 0, \tag{2.18}$$

provided nonnegative M. The Cahn-Hilliard model conserves the mass. We next discuss Allen-Cahn equations with nonlocal constraints that conserve the mass.

#### 2.3. Allen-Cahn models with nonlocal constraints

We present two methods to impose mass conservation. One is called the Allen–Cahn model with a penalizing potential and the other the Allen–Cahn model with a Lagrange multiplier. The former enforces the mass conservation approximately while the latter does it exactly.

#### 2.3.1. Allen-Cahn model with a penalizing potential

In the Allen-Cahn model with a penalizing potential model, a penalizing term is augmented to the free energy to enforce the mass conservation by the model as follows

$$F = \int_{\Omega} \left[ \frac{1}{2} \|\nabla^2 \phi\|^2 - a \|\nabla \phi\|^2 + \frac{\alpha}{2} \phi^2 + \frac{\phi^4}{4} \right] d\mathbf{r} + \frac{\eta}{2} \left( \int_{\Omega} \phi(t) d\mathbf{r} - \mathbf{M_0} \right)^2, \tag{2.19}$$

where  $\eta$  is penalizing parameter,  $\mathbf{M_0} = \int_{\Omega} \phi(0) d\mathbf{r}$  is the initial mass.

The transport equation for  $\phi$  is given by the Allen–Cahn equation

$$\frac{\partial \phi}{\partial t} = -M\tilde{\mu}, 
\frac{\partial \phi}{\partial n} = 0, \frac{\partial \nabla^2 \phi}{\partial n} = 0, \text{ in } \partial \Omega,$$
(2.20)

 $\phi|_{t=0} = \phi(0, \mathbf{x})$ 

where M is the mobility coefficient and  $ilde{\mu}$  is the chemical potential given by

$$\tilde{\mu} = \mu + \sqrt{\eta}\zeta, \quad \zeta = \sqrt{\eta} \left( \int_{\Omega} \phi(t) d\mathbf{r} - \mathbf{M_0} \right).$$
 (2.21)

The energy dissipation rate is given by

$$\frac{dF}{dt} = \int_{\Omega} \frac{\delta F}{\delta \phi} \phi_t d\mathbf{r} = \int_{\Omega} \tilde{\mu}(-M\tilde{\mu}) d\mathbf{r} \le 0, \tag{2.22}$$

provided  $M \ge 0$ . The modified Allen–Cahn equation is approximately mass preserving depending on the size of  $\eta$ . We next discuss another approach to obtain mass conservation.

#### 2.3.2. Allen-Cahn model with a Lagrange multiplier

In this model, the free energy is augmented by a penalty term with a Lagrange multiplier L as follows.

$$\tilde{F} = F - L(\int_{\Omega} \phi(t) d\mathbf{r} - \mathbf{M_0}). \tag{2.23}$$

The transport equation for  $\phi$  is given by the Allen–Cahn equation

$$\begin{split} \frac{\partial \phi}{\partial t} &= -M\tilde{\mu}, \\ \frac{\partial \phi}{\partial n} &= 0, \frac{\partial \nabla^2 \phi}{\partial n} = 0, \text{ in } \partial \Omega, \end{split} \tag{2.24}$$

 $\phi|_{t=0} = \phi(0, \mathbf{x}),$ 

where M is the mobility coefficient and  $\tilde{\mu}$  is the chemical potential given by

$$\tilde{\mu} = \mu - L, \quad L = \frac{1}{\int_{\Omega} M d\mathbf{r}} \int_{\Omega} [M\mu] d\mathbf{r}.$$
 (2.25)

The energy dissipation rate is given by

$$\frac{dF}{dt} = \int_{\Omega} \frac{\delta F}{\delta \phi} \phi_t d\mathbf{r} = \int_{\Omega} \tilde{\mu}(-M\tilde{\mu}) d\mathbf{r} \le 0, \tag{2.26}$$

provided M > 0.

#### 3. Near equilibrium dynamics of the models

To understand dynamics of the model near an equilibrium solution  $\phi^{ss}$ , we consider a small perturbation of the steady state given by  $\delta v(t, \mathbf{r})$ :

$$\phi = \phi^{ss} + \delta v. \tag{3.1}$$

For the Allen-Cahn model, substituting (3.1) into (2.14), we obtain

$$\frac{\partial \delta v}{\partial t} = -M[(\nabla^2 + a)^2 \delta v - a^2 \delta v + (\alpha + 3(\phi^{ss})^2) \delta v]. \tag{3.2}$$

We seek the solution of the linearized partial differential equation system given by

$$\delta v = \sum_{k=0}^{\infty} a_{kl} cos(kx) cos(ly), \tag{3.3}$$

in the domain  $\Omega = [-\pi, \pi]^2$ . Then, we have

$$\dot{a}_{kl}(t) = -Ma_{kl}(t)[(k^2 + l^2)^2 - 2a(k^2 + l^2) + (\alpha + 3(\phi^{ss})^2)]. \tag{3.4}$$

Instability can emerge if  $(k^2 + l^2)^2 - 2a(k^2 + l^2) + (\alpha + 3(\phi^{ss})^2) < 0$ , for some wave numbers k, l.

For the Allen–Cahn model with a penalizing potential, substituting (3.1) into the transport equation, we obtain the linearized system as follows

$$\frac{\partial \delta v}{\partial t} = -M[(\nabla^2 + a)^2 \delta v - a^2 \delta v + (\alpha + 3(\phi^{ss})^2) \delta v + \eta \int_{\Omega} \delta v d\mathbf{r}]. \tag{3.5}$$

Using ansatz (3.3), we have

$$\dot{a}_{kl(t)} = -Ma_{kl}(t)[(k^2 + l^2)^2 - 2a(k^2 + l^2) + \alpha + 3(\phi^{ss})^2 + 4\pi^2 \eta \delta_{k0} \delta_{l0}]. \tag{3.6}$$

If  $(k^2+l^2)^2-2a(k^2+l^2)+\alpha+3(\phi^{ss})^2+4\pi^2\eta\delta_{k0}\delta_{l0}<0$ , instability will occur. In comparison, the Allen–Cahn model with a penalizing potential at zero wave number is more stable than the classical Allen–Cahn model.

For the Allen–Cahn model with a Lagrange multiplier, substituting Eq. (3.1) into the transport equation, we get the linearized system

$$\frac{\partial \delta v}{\partial t} = -M[(\nabla^2 + a)^2 \delta v - a^2 \delta v + (\alpha + 3(\phi^{ss})^2) \delta v - \frac{\int_{\Omega} g'(\phi^{ss}) \delta v d\mathbf{r}}{\int_{\Omega} M d\mathbf{r}}], \tag{3.7}$$

where  $g(\phi) = M((\nabla^2 + a)^2\phi + (\alpha - a^2)\phi + \phi^3)$ . Solving the linear system using ansatz (3.3), we have

$$\dot{a}_{kl(t)} = -Ma_{kl}(t)[(k^2 + l^2)^2 - 2a(k^2 + l^2) + \alpha + 3(\phi^{ss})^2 - \frac{\int_{\Omega} M(\alpha + 3(\phi^{ss})^2) d\mathbf{r}}{\int_{\Omega} Md\mathbf{r}} \delta_{k0}\delta_{l0}].$$
(3.8)

If M is a constant and  $(k^2 + l^2)^2 - 2a(k^2 + l^2) + \alpha + 3(\phi^{ss})^2(1 - \delta_{k0}\delta_{l0}) < 0$ , instability may ensue. The contribution of the Lagrange multiplier is to introduce a destabilizing mechanism depending on steady state solution  $\phi^{ss}$ .

For the Cahn-Hilliard model, repeating the above analysis, we have the dynamical equation for the Fourier coefficients:

$$\dot{a}_{kl(t)} = -Ma_{kl}(t)[(k^2 + l^2)^2 - 2a(k^2 + l^2) + (\alpha + 3(\phi^{ss})^2)](k^2 + l^2). \tag{3.9}$$

The window of instability in the Cahn-Hilliard model is identical to that in the Allen-Cahn model. However, the two growth rates differ.

The linear stability results dictate initial transient dynamics of the solution towards or away from the given steady state. We will resort to numerical computations for long time transient behavior of the solution.

#### 4. Numerical approximations to the phase field models

We design numerical schemes to solve the above nonlocal phase field equations to ensure that the energy dissipation property as well as mass conservation are respected. We do it by employing the energy quadratization (EQ) and the scalar auxiliary variable method (SAV) developed recently [35,40,43,44]. Both methods depend on a reformulation of the models into equivalent ones with a quadratic energy. From the latter, we have effective ways to design linear numerical schemes. For a full review on EQ methods for thermodynamical models, readers are referred to a recent review article [31]. All schemes presented below are firstly given as semi-discretized ones in time and then followed by full discretizations in space. In fact, we have shown recently that BDF and Runge–Kutta methods can be used to design energy stable schemes for thermodynamical systems up to arbitrarily high order in time [38]. For comparison purposes, we also present analogous schemes for the classical Allen–Cahn and the Cahn–Hilliard model as well.

#### 4.1. Temporal discretization

#### 4.1.1. Numerical schemes for the Allen-Cahn model by EQ methods

We reformulate the free energy density by introducing an intermediate variable:

$$q = \phi^2. \tag{4.1}$$

Then, the free energy recast into

$$F = \int_{\Omega} \left[ \frac{\phi}{2} (\nabla^4 + 2a\nabla^2 + \alpha)\phi + \frac{q^2}{4} \right] d\mathbf{r}. \tag{4.2}$$

We rewrite (2.14) as

$$\frac{\partial \phi}{\partial t} = -M\mu, \quad \frac{\partial q}{\partial t} = q'\phi_t, \quad q' = \frac{\partial q}{\partial \phi}, \tag{4.3}$$

where

$$\mu = \frac{\delta F}{\delta \phi} = \nabla^4 \phi + 2a \nabla^2 \phi + \alpha \phi + \frac{1}{2} q q'. \tag{4.4}$$

We now discretize it using the linear Crank-Nicolson method in time to arrive at a second order semi-discrete scheme.

**Scheme 4.1.** Given initial conditions  $\phi^0$ ,  $q^0$ , we first compute  $\phi^1$ ,  $q^1$  by a first order scheme. Having computed  $\phi^{n-1}$ ,  $q^{n-1}$ , and  $\phi^n$ ,  $q^n$ , we compute  $\phi^{n+1}$ ,  $q^{n+1}$  as follows.

$$\phi^{n+1} - \phi^n = -\Delta t \overline{M}^{n+1/2} [(\nabla^4 \phi + 2a \nabla^2 \phi + \alpha \phi)^{n+1/2} + \frac{1}{2} q^{n+1/2} \overline{q}^{n+1/2}],$$

$$q^{n+1} - q^n = \overline{q'}^{n+1/2} (\phi^{n+1} - \phi^n),$$
(4.5)

where

$$\overline{(\bullet)}^{n+1/2} = \frac{3}{2} (\bullet)^n - \frac{1}{2} (\bullet)^{n-1}, \quad (\bullet)^{n+1/2} = \frac{1}{2} [(\bullet)^{n+1} + (\bullet)^n]. \tag{4.6}$$

The numerical implementation can be done as follows

$$\phi^{n+1} = A^{-1}b^n, q^{n+1} = q^n + \overline{q'}^{n+1/2}(\phi^{n+1} - \phi^n).$$
(4.7)

where  $A=I+\Delta t\overline{M}^{n+1/2}[\frac{\nabla^4}{2}+a\nabla^2+\frac{\alpha}{2}+\frac{(\overline{q'}^{n+1/2})^2}{4}],$   $b^n=\phi^n-\Delta t\overline{M}^{n+1/2}[\frac{\nabla^4}{2}\phi^n+a\nabla^2\phi^n+\frac{\alpha}{2}\phi^n+\frac{1}{2}q^n\overline{q'}^{n+1/2}-\frac{(\overline{q'}^{n+1/2})^2}{4}\phi^n].$  So,  $\phi^{n+1}$  is solved independent of  $q^{n+1}$ .

We define the discrete energy as follows

$$F^{n} = \int_{\Omega} \left[ \frac{\phi^{n}}{2} (\nabla^{4} + 2a\nabla^{2} + \alpha)\phi^{n} + \frac{(q^{n})^{2}}{4} \right] d\mathbf{r}.$$
 (4.8)

#### 4.1.2. Numerical schemes for the Allen-Cahn model by SAV methods

Introducing an intermediate variable  $r = \sqrt{\int_{C} \frac{\phi^4}{4} d\mathbf{r}} + C_0$  as the scalar auxiliary variable, the free energy recast into

$$F = \int_{\Omega} \left[ \frac{\phi}{2} (\nabla^4 + 2a\nabla^2 + \alpha)\phi \right] d\mathbf{r} + r^2 - C_0. \tag{4.9}$$

We rewrite (2.14) as

$$\frac{\partial \phi}{\partial t} = -M\mu, \, \mu = \frac{\delta F}{\delta \phi} = \nabla^4 \phi + 2a\nabla^2 \phi + \alpha \phi + 2rg, 
\frac{\partial r}{\partial t} = \int_{\Omega} g \phi_t d\mathbf{r}, \, g = \frac{\delta r}{\delta \phi} = \frac{\phi^3}{2\sqrt{\int_{\Omega} \frac{\phi^4}{\delta} d\mathbf{r} + C_0}}.$$
(4.10)

We then discretize it using the linear Crank-Nicolson method in time to arrive at a second order semi-discrete scheme.

**Scheme 4.2.** Given initial conditions  $\phi^0$ ,  $r^0$ , we first compute  $\phi^1$ ,  $r^1$  by a first order scheme. Having computed  $\phi^{n-1}$ ,  $r^{n-1}$ , and  $\phi^n$ ,  $r^n$ , we compute  $\phi^{n+1}$ ,  $r^{n+1}$  as follows.

$$\phi^{n+1} - \phi^n = -\Delta t \overline{M}^{n+1/2} \mu^{n+1/2},$$

$$r^{n+1} - r^n = \int_{\Omega} \overline{g}^{n+1/2} (\phi^{n+1} - \phi^n) d\mathbf{r},$$
(4.11)

where

$$\mu^{n+1/2} = \nabla^4 \phi^{n+1/2} + 2a\nabla^2 \phi^{n+1/2} + \alpha \phi^{n+1/2} + 2r^{n+1/2}\overline{g}^{n+1/2}. \tag{4.12}$$

We define the discrete energy as follows

$$F^{n} = \int_{\mathcal{Q}} \left[ \frac{\phi^{n}}{2} (\nabla^{4} + 2a\nabla^{2} + \alpha)\phi^{n} \right] d\mathbf{r} + (r^{n})^{2} - C_{0}.$$
(4.13)

The numerical scheme can be recast into

$$A\phi^{n+1} + (c, \phi^{n+1})d = b^n,$$

$$r^{n+1} - r^n = \int_{\Omega} \overline{g}^{n+1/2} (\phi^{n+1} - \phi^n) d\mathbf{r}.$$
(4.14)

where  $A=I+\Delta t\overline{M}^{n+1/2}[\frac{\nabla^4}{2}+a\nabla^2+\frac{\alpha}{2}], c=\overline{g}^{n+1/2}, d=\Delta t\overline{M}^{n+1/2}\overline{g}^{n+1/2}$  and  $b^n=\phi^n-\Delta t\overline{M}^{n+1/2}[\frac{\nabla^4}{2}\phi^n+a\nabla^2\phi^n+\frac{\alpha}{2}\phi^n+2\overline{g}^{n+1/2}r^n-\overline{g}^{n+1/2}\int_{\Omega}\overline{g}^{n+1/2}\phi^n\mathrm{d}\mathbf{r}]$ . Multiplying the inverse of A firstly and taking the inner product of the equation with c secondly, we have

$$(c, \phi^{n+1}) + (c, \phi^{n+1})(c, A^{-1}d) = (c, A^{-1}b^n). \tag{4.15}$$

Then, the solution in the scheme is solved in the following steps,

$$A[x, y] = [d, b^{n}],$$

$$\phi^{n+1} = y - \frac{(c, y)}{1 + (c, x)}x,$$

$$r^{n+1} = r^{n} + \int_{\Omega} \overline{g}^{n+1/2} (\phi^{n+1} - \phi^{n}) d\mathbf{r}.$$
(4.16)

#### 4.1.3. Numerical schemes for the Cahn-Hilliard model by EQ methods

The free energy density is reformulated by introducing an intermediate variable:

$$q = \phi^2. \tag{4.17}$$

Then, the free energy recast into

$$F = \int_{\Omega} \left[ \frac{\phi}{2} (\nabla^4 + 2a\nabla^2 + \alpha)\phi + \frac{q^2}{4} \right] d\mathbf{r}. \tag{4.18}$$

We rewrite (2.17) as

$$\frac{\partial \phi}{\partial t} = \nabla \cdot (M \nabla \mu),$$

$$\frac{\partial q}{\partial t} = q' \phi_t.$$
(4.19)

where

$$\mu = \frac{\delta F}{\delta \phi} = \nabla^4 \phi + 2a \nabla^2 \phi + \alpha \phi + \frac{1}{2} q q', \quad q' = \frac{\partial q}{\partial \phi}. \tag{4.20}$$

We then discretize it using the linear Crank-Nicolson method in time to arrive at a second order semi-discrete scheme.

**Scheme 4.3.** Given initial conditions  $\phi^0$ ,  $q^0$ , we first compute  $\phi^1$ ,  $q^1$  by a first order scheme. Having computed  $\phi^{n-1}$ ,  $q^{n-1}$ , and  $\phi^n$ ,  $q^n$ , we compute  $\phi^{n+1}$ ,  $q^{n+1}$  as follows.

$$\phi^{n+1} - \phi^{n} = \Delta t \nabla \cdot (\overline{M}^{n+1/2} \nabla [(\nabla^{4} \phi + 2a \nabla^{2} \phi + \alpha \phi)^{n+1/2} + \frac{1}{2} q^{n+1/2} \overline{q'}^{n+1/2}]),$$

$$q^{n+1} - q^{n} = \overline{q'}^{n+1/2} (\phi^{n+1} - \phi^{n}).$$
(4.21)

The discrete energy is defined as follows

$$F^{n} = \int_{\Omega} \left[ \frac{\phi^{n}}{2} (\nabla^{4} + 2a\nabla^{2} + \alpha)\phi^{n} + \frac{(q^{n})^{2}}{4} \right] d\mathbf{r}.$$
 (4.22)

The numerical implementation can be done as follows

$$\phi^{n+1} = A^{-1}b^n,$$

$$q^{n+1} = q^n + \overline{q}^{n+1/2}(\phi^{n+1} - \phi^n).$$
(4.23)

where 
$$A = I - \Delta t \nabla \cdot (\overline{M}^{n+1/2} \nabla [\frac{\nabla^4}{2} + a \nabla^2 + \frac{\alpha}{2} + \frac{(\overline{q'}^{n+1/2})^2}{4}]), b^n = \phi^n + \Delta t \nabla \cdot (\overline{M}^{n+1/2} \nabla [\frac{\nabla^4}{2} \phi^n + a \nabla^2 \phi^n + \frac{\alpha}{2} \phi^n + \frac{1}{2} q^n \overline{q'}^{n+1/2} - \frac{(\overline{q'}^{n+1/2})^2}{4} \phi^n]).$$

#### 4.1.4. Numerical schemes for the Cahn-Hilliard model by SAV methods

An intermediate variable  $r=\sqrt{\int_{\Omega}\frac{\phi^4}{4}\mathrm{d}\mathbf{r}}+C_0$  is introduced to reformulate the free energy as follows

$$F = \int_{\Omega} \left[ \frac{\phi}{2} (\nabla^4 + 2a\nabla^2 + \alpha)\phi \right] d\mathbf{r} + r^2 - C_0.$$
(4.24)

We rewrite (2.17) as

$$\frac{\partial \phi}{\partial t} = \nabla \cdot (M \nabla \mu), \quad \mu = \frac{\delta F}{\delta \phi} = \nabla^4 \phi + 2a \nabla^2 \phi + \alpha \phi + 2rg, 
\frac{\partial r}{\partial t} = \int_{\Omega} g \phi_t d\mathbf{r}, \quad g = \frac{\delta r}{\delta \phi} = \frac{\phi^3}{2\sqrt{\int_{\Omega} \frac{\phi^4}{4} d\mathbf{r} + C_0}}.$$
(4.25)

Linear Crank-Nicolson method is used in time to arrive at a second order semi-discrete scheme.

**Scheme 4.4.** Given initial conditions  $\phi^0$ ,  $r^0$ , we first compute  $\phi^1$ ,  $r^1$  by a first order scheme. Having computed  $\phi^{n-1}$ ,  $r^{n-1}$ , and  $\phi^n$ ,  $r^n$ , we compute  $\phi^{n+1}$ ,  $r^{n+1}$  as follows.

$$\phi^{n+1} - \phi^n = \Delta t \nabla \cdot (\overline{M}^{n+1/2} \nabla \mu^{n+1/2}),$$

$$r^{n+1} - r^n = \int_{\Omega} \overline{g}^{n+1/2} (\phi^{n+1} - \phi^n) d\mathbf{r},$$

$$(4.26)$$

where

$$\mu^{n+1/2} = \nabla^4 \phi^{n+1/2} + 2a\nabla^2 \phi^{n+1/2} + \alpha \phi^{n+1/2} + 2r^{n+1/2}\overline{g}^{n+1/2}. \tag{4.27}$$

The discrete energy is defined as follows

$$F^{n} = \int_{\Omega} \left[ \frac{\phi^{n}}{2} (\nabla^{4} + 2a\nabla^{2} + \alpha)\phi^{n} \right] d\mathbf{r} + (r^{n})^{2} - C_{0}.$$
(4.28)

The numerical scheme can be rewritten into

$$A\phi^{n+1} + (c, \phi^{n+1})d = b^{n},$$

$$r^{n+1} - r^{n} = \int_{\Omega} \overline{g}^{n+1/2} (\phi^{n+1} - \phi^{n}) d\mathbf{r}.$$
(4.29)

where  $A = I - \Delta t \nabla \cdot (\overline{M}^{n+1/2} \nabla [\frac{\nabla^4}{2} + a \nabla^2 + \frac{\alpha}{2}])$ ,  $c = \overline{g}^{n+1/2}$ ,  $d = \Delta t \overline{M}^{n+1/2} \overline{g}^{n+1/2}$  and  $b^n = \phi^n + \Delta t \nabla \cdot (\overline{M}^{n+1/2} \nabla [\frac{\nabla^4}{2} \phi^n + a \nabla^2 \phi^n + \frac{\alpha}{2} \phi^n + 2 \overline{g}^{n+1/2} r^n - \overline{g}^{n+1/2} \int_{\Omega} \overline{g}^{n+1/2} \phi^n d\mathbf{r}]$ ). Multiplying the first equation by the inverse of A firstly and taking the inner product of the equation with c secondly, we have

$$(c, \phi^{n+1}) + (c, \phi^{n+1})(c, A^{-1}d) = (c, A^{-1}b^n)$$
(4.30)

So we solve the solution in the scheme in the following steps,

$$A[x, y] = [d, b^{n}],$$

$$\phi^{n+1} = y - \frac{(c, y)}{1 + (c, x)}x,$$

$$r^{n+1} = r^{n} + \int_{\Omega} \overline{g}^{n+1/2} (\phi^{n+1} - \phi^{n}) d\mathbf{r}.$$
(4.31)

#### 4.1.5. Numerical schemes for the Allen-Cahn model with a penalizing potential by EQ methods

In the Allen-Cahn model with a penalizing potential, we reformulate the free energy density by introducing two intermediate variables

$$q = \phi^2, \quad \zeta = \sqrt{\eta} \left( \int_{\Omega} \phi(t) d\mathbf{r} - \mathbf{M_0} \right).$$
 (4.32)

Then, the free energy recast into

$$F = \int_{\Omega} \left[ \frac{\phi}{2} (\nabla^4 + 2a\nabla^2 + \alpha)\phi + \frac{q^2}{4} \right] d\mathbf{r} + \frac{\zeta^2}{2}. \tag{4.33}$$

We rewrite the nonlocal Allen-Cahn equation as follows:

$$\frac{\partial \phi}{\partial t} = -M\tilde{\mu}, 
\frac{\partial \zeta}{\partial t} = \sqrt{\eta} \int_{\Omega} \frac{\partial \phi}{\partial t} d\mathbf{r}, 
\frac{\partial q}{\partial t} = q' \phi_t.$$
(4.34)

where

$$\tilde{u} = u + \sqrt{\eta}\zeta, \quad \mu = \frac{\delta F}{\delta \phi} = \nabla^4 \phi + 2a\nabla^2 \phi + \alpha \phi + \frac{1}{2}qq', \quad q' = \frac{\partial q}{\partial \phi}. \tag{4.35}$$

We then discretize it using the linear Crank-Nicolson method in time to arrive at a new scheme as follows.

**Scheme 4.5.** Given initial conditions  $\phi^0$ ,  $q^0$ , we first compute  $\phi^1$ ,  $q^1$  by a first order scheme. Having computed  $\phi^{n-1}$ ,  $q^{n-1}$ , and  $\phi^n$ ,  $q^n$ , we compute  $\phi^{n+1}$ ,  $q^{n+1}$  as follows.

$$\phi^{n+1} - \phi^{n} = -\Delta t \overline{M}^{n+1/2} \tilde{\mu}^{n+1/2},$$

$$\zeta^{n+1} - \zeta^{n} = \sqrt{\eta} \int_{\Omega} (\phi^{n+1} - \phi^{n}) d\mathbf{r},$$

$$q^{n+1} - q^{n} = \overline{q}^{n+1/2} (\phi^{n+1} - \phi^{n}),$$
(4.36)

where

$$\tilde{\mu}^{n+1/2} = (\nabla^4 \phi + 2a\nabla^2 \phi + \alpha \phi)^{n+1/2} + \frac{1}{2}q^{n+1/2}\overline{q'}^{n+1/2} + \sqrt{\eta}\zeta^{n+1/2}.$$
(4.37)

The discrete energy is defined as follows

$$F^{n} = \int_{\Omega} \left[ \frac{\phi^{n}}{2} (\nabla^{4} + 2a\nabla^{2} + \alpha)\phi^{n} + \frac{(q^{n})^{2}}{4} \right] d\mathbf{r} + \frac{(\zeta^{n})^{2}}{2}.$$
(4.38)

From the scheme, it follows that

$$(I + \Delta t \overline{M}^{n+1/2} [\frac{\nabla^4}{2} + a \nabla^2 + \frac{\alpha}{2} + \frac{1}{2} (\overline{q'}^{n+1/2})^2]) \phi^{n+1} + \Delta t \overline{M}^{n+1/2} \frac{\eta}{2} \int_{\Omega} \phi^{n+1} d\mathbf{r} = b^n,$$

$$b^n = (I - \Delta t \overline{M}^{n+1/2} [\frac{\nabla^4}{2} + a \nabla^2 + \frac{\alpha}{2} + q^n \overline{q'}^{n+1/2} - \frac{1}{2} (\overline{q'}^{n+1/2})^2]) \phi^n - \sqrt{\eta} \zeta^n + \Delta t \overline{M}^{n+1/2} \frac{\eta}{2} \int_{\Omega} \phi^n d\mathbf{r}.$$
(4.39)

It can be written into a compact form,

$$A\phi^{n+1} + (c, \phi^{n+1})d = b^n, \tag{4.40}$$

where  $A=I+\Delta t\overline{M}^{n+1/2}[\frac{\nabla^4}{2}+a\nabla^2+\frac{\alpha}{2}+\frac{1}{2}(\overline{q'}^{n+1/2})^2]$ ,  $c=1, d=\frac{\Delta t\overline{M}^{n+1/2}}{2}$  and  $b^n=(I-\Delta t\overline{M}^{n+1/2}[\frac{\nabla^4}{2}+a\nabla^2+\frac{\alpha}{2}+q^n\overline{q'}^{n+1/2}-\frac{1}{2}(\overline{q'}^{n+1/2})^2])\phi^n-\sqrt{\eta}\zeta^n+\Delta t\overline{M}^{n+1/2}\frac{\eta}{2}\int_{\Omega}\phi^n\mathrm{d}\mathbf{r}$ . Then, the linear equation system is solved in the following steps,

$$A[x, y] = [d, b^{n}],$$

$$(c, \phi^{n+1}) = \frac{(c, y)}{1 + (c, x)},$$

$$\phi^{n+1} = -(c, \phi^{n+1})x + y.$$

$$(4.41)$$

4.1.6. Numerical schemes for the Allen-Cahn model with a penalizing potential by SAV methods

In the Allen-Cahn model with a penalizing potential, we reformulate the free energy density by introducing two intermediate variables

$$r = \sqrt{\int_{\Omega} \frac{\phi^4}{4} d\mathbf{r} + C_0}, \quad \zeta = \sqrt{\eta} \left( \int_{\Omega} \phi(t) d\mathbf{r} - \mathbf{M_0} \right). \tag{4.42}$$

Then, the free energy recast into

$$F = \int_{C} \left[ \frac{\phi}{2} (\nabla^4 + 2a\nabla^2 + \alpha)\phi \right] d\mathbf{r} + r^2 - C_0 + \frac{\zeta^2}{2}. \tag{4.43}$$

We rewrite the nonlocal Allen-Cahn equation as follows:

$$\frac{\partial \phi}{\partial t} = -M\tilde{\mu}, 
\frac{\partial \zeta}{\partial t} = \sqrt{\eta} \int_{\Omega} \frac{\partial \phi}{\partial t} d\mathbf{r}, 
\frac{\partial r}{\partial t} = \int_{\Omega} g \frac{\partial \phi}{\partial t} d\mathbf{r}, \tag{4.44}$$

where

$$\tilde{\mu} = \frac{\delta F}{\delta \phi} = \nabla^4 \phi + 2a \nabla^2 \phi + \alpha \phi + 2rg + \sqrt{\eta} \zeta, \quad g = \frac{\delta r}{\delta \phi} = \frac{\phi^3}{2\sqrt{\int_{\Omega} \frac{\phi^4}{4} d\mathbf{r} + C_0}}.$$
(4.45)

We then discretize it using the linear Crank-Nicolson method in time to arrive at a new scheme as follows.

**Scheme 4.6.** Given initial conditions  $\phi^0$ ,  $r^0$ , we first compute  $\phi^1$ ,  $r^1$  by a first order scheme. Having computed  $\phi^{n-1}$ ,  $r^{n-1}$ , and  $\phi^n$ ,  $r^n$ , we compute  $\phi^{n+1}$ ,  $r^{n+1}$  as follows.

$$\phi^{n+1} - \phi^{n} = -\Delta t \overline{M}^{n+1/2} \tilde{\mu}^{n+1/2},$$

$$\zeta^{n+1} - \zeta^{n} = \sqrt{\eta} \int_{\Omega} (\phi^{n+1} - \phi^{n}) d\mathbf{r},$$

$$r^{n+1} - r^{n} = \int_{\Omega} \overline{g}^{n+1/2} (\phi^{n+1} - \phi^{n}) d\mathbf{r},$$
(4.46)

where

$$\tilde{\mu}^{n+1/2} = \mu^{n+1/2} + \sqrt{\eta} \zeta^{n+1/2}, \mu^{n+1/2} = (\nabla^4 \phi + 2a \nabla^2 \phi + \alpha \phi)^{n+1/2} + 2r^{n+1/2} \overline{g}^{n+1/2}.$$
(4.47)

The discrete energy is defined as follows

$$F^{n} = \int_{\mathcal{O}} \left[ \frac{\phi^{n}}{2} (\nabla^{4} + 2a\nabla^{2} + \alpha)\phi^{n} \right] d\mathbf{r} + (r^{n})^{2} + \frac{(\zeta^{n})^{2}}{2} - C_{0}.$$
(4.48)

The scheme can be recast into

$$A\phi^{n+1} + (\phi^{n+1}, c_1)d_1 + (\phi^{n+1}, c_2)d_2 = b^n, \tag{4.49}$$

where

$$A = I + \Delta t \overline{M}^{n+1/2} \left[ \frac{\nabla^{4}}{2} + a \nabla^{2} + \frac{\alpha}{2} \right],$$

$$c_{1} = \overline{g}^{n+1/2},$$

$$d_{1} = \Delta t \overline{M}^{n+1/2} \overline{g}^{n+1/2},$$

$$c_{2} = 1, \ d_{2} = \frac{\Delta t \overline{M}^{n+1/2}}{2} \eta,$$

$$b^{n} = \phi^{n} - \Delta t \overline{M}^{n+1/2} \left[ \frac{\nabla^{2}}{2} \phi^{n} + a \nabla^{2} \phi^{n} + \frac{\alpha}{2} \phi^{n} + 2 r^{n} \overline{g}^{n+1/2} - \overline{g}^{n+1/2} \right]$$

$$\overline{g}^{n+1/2} \int_{\Omega} \overline{g}^{n+1/2} \phi^{n} d\mathbf{r} - \Delta t \overline{M}^{n+1/2} \sqrt{\eta} \zeta^{n} + \Delta t \overline{M}^{n+1/2} \frac{\eta}{2} \int_{\Omega} \phi^{n} d\mathbf{r}.$$
(4.50)

It implies that

$$(\phi^{n+1}, c_1) + (\phi^{n+1}, c_1)(A^{-1}d_1, c_1) + (\phi^{n+1}, c_2)(A^{-1}d_2, c_1) = (A^{-1}b^n, c_1),$$

$$(\phi^{n+1}, c_2) + (\phi^{n+1}, c_1)(A^{-1}d_1, c_2) + (\phi^{n+1}, c_2)(A^{-1}d_2, c_2) = (A^{-1}b^n, c_2).$$

$$(4.51)$$

We solve for  $(\phi^{n+1}, c_1)$  and  $(\phi^{n+1}, c_2)$  from the above equation after we obtain

$$A[x, y, z] = [d_1, d_2, b^n]. (4.52)$$

So, the solution is solved in the following steps,

$$\phi^{n+1} = z - [(\phi^{n+1}, c_1)x + (\phi^{n+1}, c_2)y],$$

$$r^{n+1} = r^n + (\phi^{n+1} - \phi^n, \frac{\overline{g}^{n+1/2}}{2}),$$

$$\zeta^{n+1} = \zeta^n + \sqrt{\eta}((\phi^{n+1}, 1) - (\phi^n, 1)).$$
(4.53)

4.1.7. Numerical schemes for the Allen-Cahn model with a Lagrange multiplier by EQ methods We reformulate the free energy density by introducing an intermediate variable

$$q = \phi^2. \tag{4.54}$$

Then, the free energy recast into

$$F = \int_{\Omega} \left[ \frac{\phi}{2} (\nabla^4 + 2a\nabla^2 + \alpha)\phi + \frac{q^2}{4} \right] d\mathbf{r} - L \left( \int_{\Omega} \phi(t) d\mathbf{r} - \int_{\Omega} \phi(0) d\mathbf{r} \right). \tag{4.55}$$

We rewrite (2.24) as

$$\frac{\partial \phi}{\partial t} = -M\tilde{\mu}, \quad \frac{\partial q}{\partial t} = q'\phi_t, \tag{4.56}$$

where

$$\tilde{\mu} = \frac{\delta F}{\delta \phi} = \nabla^4 \phi + 2a \nabla^2 \phi + \alpha \phi + \frac{1}{2} q q' - L, \quad L = \frac{1}{\int_{\Omega} M d\mathbf{r}} \int_{\Omega} M \tilde{\mu} d\mathbf{r}, \quad q' = \frac{\partial q}{\partial \phi}. \tag{4.57}$$

We then discretize it using the linear modified Crank-Nicolson method in time as follows.

**Scheme 4.7.** Given initial conditions  $\phi^0$ ,  $q^0$ , we first compute  $\phi^1$ ,  $q^1$  by a first order scheme. Having computed  $\phi^{n-1}$ ,  $q^{n-1}$ , and  $\phi^n$ ,  $q^n$ , we compute  $\phi^{n+1}$ ,  $q^{n+1}$  as follows.

$$\phi^{n+1} - \phi^n = -\Delta t \overline{M}^{n+1/2} \tilde{\mu}^{n+1/2},$$

$$q^{n+1} - q^n = \overline{q'}^{n+1/2} (\phi^{n+1} - \phi^n).$$
(4.58)

where

$$\tilde{\mu}^{n+1/2} = (\nabla^4 \phi + 2a \nabla^2 \phi + \alpha \phi)^{n+1/2} + \frac{1}{2} q^{n+1/2} \overline{q'}^{n+1/2} - L^{n+1/2},$$

$$L^{n+1/2} = \frac{1}{\int_{\Omega} \overline{M}^{n+1/2} d\mathbf{r}} \int_{\Omega} \overline{M}^{n+1/2} \mu^{n+1/2} d\mathbf{r}.$$
(4.59)

**Remark.**  $L^{n+1/2} \neq \frac{L^n + L^{n+1}}{2}$ 

Then, we have the following theorem

**Theorem 4.1.** The mass of each phase is conserved, i.e.,

$$\int_{\Omega} \phi^{n+1} d\mathbf{r} = \int_{\Omega} \phi^{n} d\mathbf{r}. \tag{4.60}$$

**Proof.** Substituting the  $L^{n+1/2}$  into the equation below, we have

$$\int_{\Omega} \frac{\phi^{n+1} - \phi^{n}}{\Delta t} d\mathbf{r} 
= \int_{\Omega} -\overline{M}^{n+1/2} (\mu^{n+1/2} - L^{n+1/2}) d\mathbf{r} = 0.$$
(4.61)

This implies the mass-conservation property.

We define the discrete energy as follows

$$F^{n} = \int_{\mathcal{Q}} \left[ \frac{\phi^{n}}{2} (\nabla^{4} + 2a\nabla^{2} + \alpha)\phi^{n} + \frac{(q^{n})^{2}}{4} \right] d\mathbf{r}.$$
 (4.62)

The solution is solved in the following steps

$$A[x, y] = [d, b^{n}],$$

$$(\phi^{n+1}, c) = \frac{(y, c)}{1 + (x, c)},$$

$$\phi^{n+1} = y - (\phi^{n+1}, c)x,$$

$$q^{n+1} = q^{n} + \overline{q}^{n+1/2}(\phi^{n+1} - \phi^{n}),$$

$$(4.63)$$

where

$$A = I + \Delta t \overline{M}^{n+1/2} \left[ \frac{\nabla^{4}}{2} + a \nabla^{2} + \frac{\alpha}{2} + \frac{1}{4} (\overline{q'}^{n+1/2})^{2} \right],$$

$$c = \overline{M}^{n+1/2} \left[ \frac{\nabla^{4}}{2} + a \nabla^{2} + \frac{\alpha}{2} + \frac{1}{4} (\overline{q'}^{n+1/2})^{2} \right],$$

$$d = -\frac{\Delta t \overline{M}^{n+1/2}}{\int_{\Omega} \overline{M}^{n+1/2} d\mathbf{r}},$$

$$b^{n} = \phi^{n} - \Delta t \overline{M}^{n+1/2} \left( \frac{\nabla^{4}}{2} \phi^{n} + a \nabla^{2} \phi^{n} + \frac{\alpha}{2} \phi^{n} + \frac{1}{2} q^{n} \overline{q'}^{n+1/2} - \frac{1}{4} (\overline{q'}^{n+1/2})^{2} \phi^{n} - \frac{\int_{\Omega} \overline{M}^{n+1/2} (\frac{\nabla^{4}}{2} \phi^{n} + a \nabla^{2} \phi^{n} + \frac{\alpha}{2} \phi^{n} + \frac{1}{2} q^{n} \overline{q'}^{n+1/2} - \frac{1}{4} (\overline{q'}^{n+1/2})^{2} \phi^{n}) d\mathbf{r}}{\int_{\Omega} \overline{M}^{n+1/2} d\mathbf{r}}$$

$$(4.64)$$

4.1.8. Numerical schemes for the Allen-Cahn model with Lagrange multipliers by SAV methods We reformulate the free energy density by introducing an intermediate variable

$$r = \sqrt{\int_{\Omega} \frac{\phi^4}{4} d\mathbf{r} + C_0}.$$
 (4.65)

Then, the free energy recast into

$$F = \int_{\Omega} \left[ \frac{\phi}{2} (\nabla^4 + 2a\nabla^2 + \alpha)\phi \right] d\mathbf{r} + r^2 - C_0 - L(\int_{\Omega} \phi(t) d\mathbf{r} - \int_{\Omega} \phi(0) d\mathbf{r}). \tag{4.66}$$

We rewrite (2.24) as

$$\frac{\partial \phi}{\partial t} = -M\tilde{\mu}, \quad \frac{\partial r}{\partial t} = \int_{\Omega} g\phi_t d\mathbf{r}, \tag{4.67}$$

where

$$\tilde{\mu} = \frac{\delta F}{\delta \phi} = \nabla^4 \phi + 2a\nabla^2 \phi + \alpha \phi + 2rg - L, \quad L = \frac{1}{\int_{\Omega} M d\mathbf{r}} \int_{\Omega} M \mu d\mathbf{r}, \quad g = \frac{\partial r}{\partial \phi} = \frac{\phi^3}{2\sqrt{\int_{\Omega} \frac{\phi^4}{\phi^4} d\mathbf{r} + C_0}}.$$
 (4.68)

We then discretize it using the modified Crank-Nicolson method in time as follows.

**Scheme 4.8.** Given initial conditions  $\phi^0$ ,  $r^0$ , we first compute  $\phi^1$ ,  $r^1$  by a first order scheme. Having computed  $\phi^{n-1}$ ,  $r^{n-1}$ , and  $\phi^n$ ,  $r^n$ , we compute  $\phi^{n+1}$ ,  $r^{n+1}$  as follows.

$$\phi^{n+1} - \phi^n = -\Delta t \overline{M}^{n+1/2} [(\nabla^4 \phi + 2a \nabla^2 \phi + \alpha \phi)^{n+1/2} + 2r^{n+1/2} \overline{g}^{n+1/2} - L^{n+1/2}],$$

$$r^{n+1} - r^n = \int_{\Omega} \overline{g}^{n+1/2} (\phi^{n+1} - \phi^n) d\mathbf{r}.$$
(4.69)

where

$$\tilde{\mu}^{n+1/2} = (\nabla^4 \phi + 2a \nabla^2 \phi + \alpha \phi)^{n+1/2} + 2r^{n+1/2} \overline{g}^{n+1/2} - L^{n+1/2},$$

$$L^{n+1/2} = \frac{1}{\int_{\Omega} \overline{M}^{n+1/2} d\mathbf{r}} \int_{\Omega} \overline{M}^{n+1/2} \mu^{n+1/2} d\mathbf{r}.$$
(4.70)

Then, we have the following theorem

**Theorem 4.2.** The mass of each phase is conserved, i.e.,

$$\int_{\Omega} \phi^{n+1} d\mathbf{r} = \int_{\Omega} \phi^{n} d\mathbf{r}.$$
(4.71)

**Proof.** The proof is similar to that of Theorem 4.1 and is thus omitted.

We define the discrete energy as follows

$$F^{n} = \int_{\Omega} \left[ \frac{\phi^{n}}{2} (\nabla^{4} + 2a\nabla^{2} + \alpha)\phi^{n} \right] d\mathbf{r} + (r^{n})^{2} - C_{0}.$$
(4.72)

This scheme can be recast into

$$A\phi^{n+1} + (\phi^{n+1}, c_1)d_1 + (\phi^{n+1}, c_2)d_2 + (c_3, (\phi^{n+1}, c_1))d_2 = b^n,$$

$$(4.73)$$

So we have

$$(\phi^{n+1}, c_1) + (\phi^{n+1}, c_1)(A^{-1}d_1, c_1) + (\phi^{n+1}, c_2)(A^{-1}d_2, c_1) + (c_3, (\phi^{n+1}, c_1))(A^{-1}d_2, c_1) = (A^{-1}b^n, c_1),$$
 
$$(\phi^{n+1}, c_2) + (\phi^{n+1}, c_1)(A^{-1}d_1, c_2) + (\phi^{n+1}, c_2)(A^{-1}d_2, c_2) + (c_3, (\phi^{n+1}, c_1))(A^{-1}d_2, c_2) = (A^{-1}b^n, c_2).$$
 
$$(4.74)$$

We solve for  $(\phi^{n+1}, c_1)$  and  $(\phi^{n+1}, c_2)$  from the above equations after we obtain

$$A[x, y, z] = [d_1, d_2, b^n], \tag{4.75}$$

where

$$A = I + \Delta t \overline{M}^{n+1/2} \left( \frac{\nabla^{4}}{2} + a \nabla^{2} + \frac{\alpha}{2} \right),$$

$$c_{1} = \overline{g}^{n+1/2}, d_{1} = \Delta t \overline{M}^{n+1/2} \overline{g}^{n+1/2},$$

$$c_{2} = \overline{M}^{n+1/2} \left( \frac{\nabla^{4}}{2} + a \nabla^{2} + \frac{\alpha}{2} \right),$$

$$d_{2} = -\Delta t \overline{M}^{n+1/2} \frac{1}{\int_{\Omega} \overline{M}^{n+1/2} d\mathbf{r}},$$

$$c_{3} = \overline{M}^{n+1/2},$$

$$b^{n} = \phi^{n} - \Delta t \overline{M}^{n+1/2} \left( \frac{\nabla^{4}}{2} \phi^{n} + a \nabla^{2} \phi^{n} + \frac{\alpha}{2} \phi^{n} + 2r^{n} \overline{g}^{n+1/2} - \overline{g}^{n+1/2} \int_{\Omega} \overline{g}^{n+1/2} \phi^{n} d\mathbf{r} \right)$$

$$-(\overline{M}^{n+1/2}, \frac{\nabla^{4}}{2} \phi^{n} + a \nabla^{2} \phi^{n} + \frac{\alpha}{2} \phi^{n} + 2r^{n} \overline{g}^{n+1/2} - \overline{g}^{n+1/2} \int_{\Omega} \overline{g}^{n+1/2} \phi^{n} d\mathbf{r}) d_{2}.$$

$$(4.76)$$

Finally, the solution is obtained as follows

$$A[x, y, z] = [d_1, d_2, b^n],$$

$$\phi^{n+1} = z - (\phi^{n+1}, c_1)x - (\phi^{n+1}, c_2)y - (c_3, (\phi^{n+1}, c_1))y,$$

$$r^{n+1} = r^n + (\overline{g}^{n+1/2}, (\phi^{n+1} - \phi^n)).$$
(4.77)

#### 4.2. Spatial discretization

We use the finite difference method to discretize the equations with the Neumann boundary condition in space for all models. The linear spatially dependent PDE systems resulting from all semi-discrete schemes are spatially discretized by compact second order finite difference methods at the cell center. We divide the 2D domain  $\Omega = [0, L_x] \times [0, L_y]$  into rectangular meshes with mesh sizes  $h_x = L_x/N_x$  and  $h_y = L_y/N_y$ , where  $L_x$ ,  $L_y$  are two positive real numbers and  $N_x$ ,  $N_y$  are the number of meshes in each direction. After this, the sets of the cell center points  $C_x$  and  $C_y$  for the uniform partition are defined as follows

$$C_x = \{x_i | i = 0, 1, \dots, N_x\}, \quad C_y = \{y_j | j = 0, 1, \dots, N_y\},$$
 (4.78)

where  $x_i = (i - \frac{1}{2})h_x$  and  $y_j = (j - \frac{1}{2})h_y$ . We define the east–west-edge-to-center and center-to-east–west-edge difference operators  $d_x$  and  $D_x$  as follows

$$d_{x}\phi_{ij} = \frac{\phi_{i+\frac{1}{2},j} - \phi_{i-\frac{1}{2},j}}{h_{x}}, \qquad D_{x}\phi_{i+\frac{1}{2},j} = \frac{\phi_{i+1,j} - \phi_{i-1,j}}{h_{x}}.$$
(4.79)

Similarly, we define the north-south-edge-to-center and center-to-north-south-edge difference operators  $d_v$  and  $D_v$  as follows

$$d_y \phi_{ij} = \frac{\phi_{i,j+\frac{1}{2}} - \phi_{i,j-\frac{1}{2}}}{h_v}, \qquad D_y \phi_{i,j+\frac{1}{2}} = \frac{\phi_{i,j+1} - \phi_{i,j-1}}{h_v}. \tag{4.80}$$

The fully discrete Laplacian and fourth order gradient operator are given by

$$\nabla_{h}^{2} = \Delta_{h} = d_{X}(D_{X}\phi) + d_{Y}(D_{Y}\phi), \quad \nabla_{h}^{4} = \Delta_{h}^{2} = d_{X}(D_{X}\Delta_{h}) + d_{Y}(D_{Y}\Delta_{h}). \tag{4.81}$$

The discrete inner product is defined as follows

$$\langle f, g \rangle = h_x h_y \sum_{i,j} f_{i,j} g_{i,j}, \tag{4.82}$$

where  $f_{ij}$  and  $g_{ij}$  are given at the cell center. In particular,

$$\langle f, 1 \rangle = h_{\mathsf{x}} h_{\mathsf{y}} \sum_{i,j} f_{i,j}, \quad \|f\|_{d} = \sqrt{\langle f, f \rangle}. \tag{4.83}$$

With the notations, we replace the continuous differential operators in the semi-discrete schemes by the discrete difference operators to arrive at the corresponding fully discrete schemes. To save space, we will not enumerate them here.

#### 4.3. Energy dissipation property and solvability of the linear systems resulting from the schemes

We summarize the energy dissipation law and unique solvability for all linear systems resulting from the semidiscrete schemes presented in this section into two theorems. The proofs of the energy dissipation property and solvability for the fully discrete schemes are similar, we only prove the theorems for the Allen–Cahn model with a Lagrange multiplier discretized using EQ methods below and omit others for simplicity. Based on Scheme 4.7 and the spatial discretization, the fully discrete scheme corresponding to Scheme 4.7 is summarized below.

**Scheme 4.9.** Given initial conditions  $\phi^0$ ,  $q^0$ , we first compute  $\phi^1$ ,  $q^1$  by a first order scheme. Having computed  $\phi^{n-1}$ ,  $q^{n-1}$ , and  $\phi^n$ ,  $q^n$ , we compute  $\phi^{n+1}$ ,  $q^{n+1}$  as follows.

$$\phi^{n+1} - \phi^{n} - \Delta t \overline{M}^{n+1/2} [(\nabla_{h}^{4} \phi + 2a \nabla_{h}^{2} \phi + \alpha \phi)^{n+1/2} + \frac{1}{2} q^{n+1/2} \overline{q'}^{n+1/2} - L^{n+1/2}],$$

$$q^{n+1} - q^{n} = \overline{q'}^{n+1/2} (\phi^{n+1} - \phi^{n}).$$
(4.84)

where

$$\tilde{\mu}^{n+1/2} = (\nabla_h^4 \phi + 2a \nabla_h^2 \phi + \alpha \phi)^{n+1/2} + \frac{1}{2} q^{n+1/2} \overline{q'}^{n+1/2} - L^{n+1/2},$$

$$L^{n+1/2} = \frac{1}{\int_{\Omega} \overline{M}^{n+1/2} d\mathbf{r}} \int_{\Omega} \overline{M}^{n+1/2} \mu^{n+1/2} d\mathbf{r}.$$
(4.85)

We define the discrete energy as follows

$$F^{n} = \langle \frac{\phi^{n}}{2} (\nabla_{h}^{4} + 2a\nabla_{h}^{2} + \alpha)\phi^{n} + \frac{(q^{n})^{2}}{4}, 1 \rangle.$$
 (4.86)

Theorem 4.3. The fully discrete scheme obeys the following energy dissipation law

$$F^{n+1} - F^n = -\Delta t \langle \mu^{n+1/2} - L^{n+1/2}, \overline{M}^{n+1/2} (\mu^{n+1/2} - L^{n+1/2}) \rangle. \tag{4.87}$$

**Proof.** Taking inner product of (4.84) with  $-u^{n+1/2}$ , we obtain

$$-\langle \frac{\phi^{n+1} - \phi^{n}}{\Delta t}, \mu^{n+1/2} \rangle 
= -\langle -\overline{M}^{n+1/2} [\mu^{n+1/2} - L^{n+1/2}], \mu^{n+1/2} \rangle 
= \|\sqrt{\overline{M}^{n+1/2}} (\mu^{n+1/2} - L^{n+1/2})\|_{d}^{2} + \langle \overline{M}^{n+1/2} [\mu^{n+1/2} - L^{n+1/2}], L^{n+1/2} \rangle.$$
(4.88)

Taking inner product of  $\mu^{n+1/2}$  with  $\frac{\phi^{n+1}-\phi^n}{\Delta t}$ , we have

$$\langle (\nabla_{h}^{4}\phi + 2a\nabla_{h}^{2}\phi + \alpha\phi)^{n+1/2} + \frac{1}{2}q^{n+1/2}\overline{q'}^{n+1/2}, \frac{\phi^{n+1} - \phi^{n}}{\Delta t} \rangle \\
= \frac{\|\nabla_{h}^{2}\phi^{n+1}\|_{d}^{2} - \|\nabla_{h}^{2}\phi^{n}\|_{d}^{2}}{2\Delta t} - a\frac{\|\nabla_{h}\phi^{n+1}\|_{d}^{2} - \|\nabla_{h}\phi^{n}\|_{d}^{2}}{\Delta t} + \frac{\alpha}{2\Delta t}(\|\phi^{n+1}\|_{d}^{2} - \|\phi^{n}\|_{d}^{2}) + \langle \frac{1}{2}q^{n+1/2}\overline{q'}^{n+1/2}, \frac{\phi^{n+1} - \phi^{n}}{\Delta t} \rangle.$$
(4.89)

Taking inner product of  $q^{n+1}-q^n$  with  $\frac{q^{n+1}+q^n}{\Delta t}$ , we obtain

$$\frac{1}{\Delta t}(\|q^{n+1}\|_d^2 - \|q^n\|_d^2) = \frac{1}{\Delta t} \langle \overline{q'}^{n+1/2}(\phi^{n+1} - \phi^n), q^{n+1} + q^n \rangle. \tag{4.90}$$

Combining the above equations, we obtain

$$\begin{split} &\frac{\|\nabla_{h}^{2}\phi^{n+1}\|_{d}^{2} - \|\nabla_{h}^{2}\phi^{n}\|_{d}^{2}}{2\Delta t} - a\frac{\|\nabla_{h}\phi^{n+1}\|_{d}^{2} - \|\nabla_{h}\phi^{n}\|_{d}^{2}}{\Delta t} + \frac{\alpha}{2\Delta t}(\|\phi^{n+1}\|_{d}^{2} - \|\phi^{n}\|_{d}^{2}) + \frac{1}{4\Delta t}(\|q^{n+1}\|_{d}^{2} - \|q^{n}\|_{d}^{2}) \\ &= -\|\sqrt{\overline{M}}^{n+1/2}(\mu^{n+1/2} - L^{n+1/2})\|_{d}^{2} - (\overline{M}^{n+1/2}[\mu^{n+1/2} - L^{n+1/2}], L^{n+1/2}). \end{split} \tag{4.91}$$

Substituting the expression of  $L^{n+1/2}$  into the equation, we have

$$-\|\sqrt{\overline{M}^{n+1/2}}(\mu^{n+1/2} - L^{n+1/2})\|_{d}^{2} - (\overline{M}^{n+1/2}[\mu^{n+1/2} - L^{n+1/2}], L^{n+1/2})$$

$$= -\|\sqrt{\overline{M}^{n+1/2}}(\mu^{n+1/2} - L^{n+1/2})\|_{d}^{2}.$$
(4.92)

**Remark.** (i). This proof applies to the semi-discrete schemes as well. (ii). When the linear schemes of the nonlocal Allen–Cahn model involve integrals discretized by a composite Trapezoidal rule, efficient numerical methods can be devised to solve the resulting linear systems. Such methods are derived from the Sherman–Morrison formula (See Appendix).

**Theorem 4.4.** The linear system resulting from the above fully discrete scheme admits a unique solution at sufficiently small  $\Delta t > 0$ .

**Proof.** Note that the solution in scheme (4.84) is solved via the following steps

$$A\phi^{n+1} + (\phi^{n+1}, c)d = b^n, \quad q^{n+1} - q^n = \overline{q'}^{n+1/2}(\phi^{n+1} - \phi^n), \tag{4.93}$$

where

$$A = I + \Delta t \overline{M}^{n+1/2} \left[ \frac{\nabla_{h}^{4}}{2} + a \nabla_{h}^{2} + \frac{\alpha}{2} + \frac{1}{4} (\overline{q'}^{n+1/2})^{2} \right],$$

$$c = \overline{M}^{n+1/2} \left[ \frac{\nabla_{h}^{4}}{2} + a \nabla_{h}^{2} + \frac{\alpha}{2} + \frac{1}{4} (\overline{q'}^{n+1/2})^{2} \right],$$

$$d = -\frac{\Delta t \overline{M}^{n+1/2}}{\langle \sqrt{\overline{M}^{n+1/2}}, \sqrt{\overline{M}^{n+1/2}} \rangle},$$

$$b^{n} = \phi^{n} - \Delta t \overline{M}^{n+1/2} \left( \frac{\nabla_{h}^{4}}{2} \phi^{n} + a \nabla_{h}^{2} \phi^{n} + \frac{\alpha}{2} \phi^{n} + \frac{q^{n} \overline{q'}^{n+1/2}}{2} - \frac{1}{4} (\overline{q'}^{n+1/2})^{2} \phi^{n} - \frac{\langle \overline{M}^{n+1/2}, \frac{\nabla_{h}^{4}}{2} \phi^{n} + a \nabla_{h}^{2} \phi^{n} + \frac{q^{n} \overline{q'}^{n+1/2}}{2} - \frac{1}{4} (\overline{q'}^{n+1/2})^{2} \phi^{n} \rangle}{\langle \sqrt{\overline{M}^{n+1/2}}, \sqrt{\overline{M}^{n+1/2}}, \sqrt{\overline{M}^{n+1/2}} \rangle}.$$

$$(4.94)$$

From the Sherman–Morrison formula, we notice that the solution uniqueness of  $A\phi^{n+1} + (\phi^{n+1}, c)d = b^n$  depends on the uniqueness of the corresponding linear system  $A\phi^{n+1} = b^n$ . Now we only need to prove the uniqueness of the solution for

$$A\phi^{n+1} = \mathbf{0}.\tag{4.95}$$

If  $\Delta t$  is small enough, we have

$$\langle A\phi, \phi \rangle = \langle \phi, A\phi \rangle = \langle \phi, (I + \Delta t \overline{M} [\frac{\nabla_h^4}{2} + a \nabla_h^2 + \frac{\alpha}{2} + \frac{1}{4} (\overline{q'})^2]) \phi \rangle$$

$$= \langle \phi, \phi \rangle + \langle \phi, \Delta t \overline{M} \frac{\nabla_h^4}{2} \phi \rangle + \langle \phi, \Delta t \overline{M} a \nabla_h^2 \phi \rangle$$

$$+ \langle \phi, \Delta t \overline{M} \frac{\alpha}{2} \phi \rangle + \langle \phi, \Delta t \overline{M} \frac{1}{4} (\overline{q'})^2 \phi \rangle$$

$$> 0. \tag{4.96}$$

So,  $A\phi = 0$  has only zero solution.

**Remark.** One can prove the uniqueness of the solution for any time step size if  $\mu^{n+1/2} = \nabla_h^4 \phi^{n+1/2} + 2a\nabla_h^2 \overline{\phi}^{n+1/2} + \alpha \phi^{n+1/2} + \frac{1}{2}q^{n+1/2} \overline{q}^{n+1/2}$  in Eq. (4.84). This discretization of the chemical potential also yields a second order unconditional energy stable scheme.

#### 5. Numerical results and discussions

In this section, we conduct mesh refinement tests to validate the accuracy of the proposed schemes and then present some numerical examples to assess the schemes for the nonlocal Allen–Cahn models against those for the Cahn–Hilliard model. For convenience, we refer the numerical schemes designed by EQ methods for the Allen–Cahn model, the Cahn–Hilliard model, the Allen–Cahn model with a penalizing potential and the Allen–Cahn model with a Lagrange multiplier as AC-EQ, CH-EQ, AC-P-EQ and AC-L-EQ, respectively. Similarly, we name the numerical schemes obtained using SAV approaches for the models as AC-SAV, CH-SAV, AC-P-SAV, AC-L-SAV, respectively. In the following, we set the constant in the free energy at  $C_0 = 1 \times 10^4$  in all computations.

#### 5.1. Mesh refinement test

We confirm the convergence rates of the proposed schemes for the PFC models through mesh refinement tests. The computational domain is set as  $\Omega = [0, 1]^2$ . The model parameter values are chosen as a = 1,  $\varepsilon = 0.1$ ,  $M = 1 \times 10^{-3}$ .

**Table 1**Mesh refinement tests in time for the proposed schemes using EQ methods.

Scheme		AC-EQ		CH-EQ		AC-P-EQ		AC-L-EQ	
Coarse $\Delta t$	Fine $\Delta t$	L <sup>2</sup> error	Order						
5.00E-02	2.5E-2	1.21E-06	_	1.23E-05	_	1.21E-06	_	1.21E-06	_
2.5E-2	1.25E-2	3.02E-07	2.00	3.12E-06	1.98	3.02E - 07	2.00	3.02E - 07	2.00
1.25E-2	6.25E-3	7.56E-08	2.00	7.84E-07	1.99	7.56E-08	2.00	7.56E-08	2.00
6.25E-3	3.125E-3	1.89E-08	2.00	1.96E-07	2.00	1.89E-08	2.00	1.89E-08	2.00
3.125E-3	1.5625E-3	4.72E-09	2.00	4.90E-08	2.00	4.72E-09	2.00	4.72E-09	2.00

 Table 2

 Mesh refinement tests in time for the proposed schemes using SAV methods.

Scheme		AC-SAV		CH-SAV		AC-P-SAV		AC-L-SAV	
Coarse ∆t	Fine <i>∆t</i>	L <sup>2</sup> error	Order						
5.00E-02	2.5E-2	1.24E-06	_	1.22E-05	_	1.24E-06	_	1.24E-06	_
2.5E-2	1.25E-2	3.09E-07	2.00	3.10E-06	1.98	3.09E-07	2.00	3.09E-07	2.00
1.25E-2	6.25E-3	7.72E - 08	2.00	7.78E-07	1.99	7.72E - 08	2.00	7.72E - 08	2.00
6.25E - 3	3.125E-3	1.93E-08	2.00	1.95E-07	2.00	1.93E-08	2.00	1.93E-08	2.00
3.125E-3	1.5625E-3	4.83E-09	2.00	4.87E-08	2.00	4.82E-09	2.00	4.82E-09	2.00

Table 3
Mesh refinement tests in space for the proposed schemes using EQ methods.

Scheme		AC-EQ		CH-EQ		AC-P-EQ		AC-L-EQ	
Coarse δt	Fine $\delta t$	L <sup>2</sup> error	Order						
1/8	1/16	3.39E-03	-	3.39E-03	-	3.39E-03	-	6.06E-05	-
1/16	1/32	8.492E-04	2.00	8.492E-04	2.00	8.492E-04	2.00	1.36E-05	2.16
1/32	1/64	2.12E-04	2.00	2.12E-04	2.00	2.12E-04	2.00	3.31E-06	2.04
1/64	1/128	5.31E-05	2.00	5.31E-05	2.00	5.31E-05	2.00	8.21E-07	2.01
1/128	1/256	1.33E-05	2.00	1.33E-05	2.00	1.33E-05	2.00	2.05E-07	2.00

**Table 4**Mesh refinement tests in space for the proposed schemes using SAV methods.

Scheme		AC-SAV		CH-SAV		AC-P-SAV		AC-L-SAV	
Coarse $\delta t$	Fine $\delta t$	$L^2$ error	Order	$L^2$ error	Order	$L^2$ error	Order	L <sup>2</sup> error	Order
1/8	1/16	3.39E-03	_	3.39E-03	_	3.39E-03	_	6.06E-05	-
1/16	1/32	8.492E-04	2.00	8.492E-04	2.00	8.492E - 04	2.00	1.36E-05	2.16
1/32	1/64	2.12E-04	2.00	2.12E-04	2.00	2.12E-04	2.00	3.31E-06	2.04
1/64	1/128	5.31E-05	2.00	5.31E-05	2.00	5.31E-05	2.00	8.21E-07	2.01
1/128	1/256	1.33E-05	2.00	1.33E-05	2.00	1.33E-05	2.00	2.05E-07	2.00

**Table 5** Efficiency of the schemes at 1000 time steps with respect to M = 0.001, 1 and 100 (from top to below).

Scheme	AC-EQ	AC-SAV	CH-EQ	CH-SAV	AC-P-EQ	AC-P-SAV	AC-L-EQ	AC-L-SAV
Time (s)	45.3	77.9	66.0	107.8	68.3	90.0	110.0	103.2
Time (s)	44.4	76	54.6	104	38.8	84.2	53.9	100.7
Time (s)	53.4	75.0	66.8	111.9	61.4	83.2	103.3	99.5

We solve the equations with the initial condition given by

$$\phi(0, x, y) = \frac{1}{2} + \frac{1}{2}\cos(\pi x)\cos(\pi y). \tag{5.1}$$

We choose the space step size  $h_x = h_y = \frac{1}{256}$ . By taking a linear refinement path  $\Delta t = \frac{0.05}{2^k}$ ,  $k = 0, 1, \dots, 5$ , we calculate the  $L^2$  errors of the phase variable with adjacent k at t = 1. The tables show the schemes are second order accurate in time numerically (see Tables 1 and 2). Besides this, we also take a linear refinement path  $\Delta h = \frac{1}{2^{3+1}}$ ,  $l = 0, 1, \dots, 5$  to test the accuracy in space numerically. Tables 3 and 4 show the schemes are also second order accurate in space.

We also compare the computational efficiency of all schemes designed by EQ and SAV methods with  $M=1\times 10^{-3}$ , 1 and  $1\times 10^2$  in Table 5. The AC-P-EQ/SAV schemes perform the best among the schemes for nonlocal Allen–Cahn models. Besides this, AC-P-EQ/SAV schemes also perform better than CH-EQ/SAV schemes in most test cases. In fact, the accuracy of the Cahn–Hilliard model relies on the mobility coefficient M more sensitively than the Allen–Cahn models do. Hence, the accuracy of the schemes for the nonlocal Allen–Cahn models is better than that for the Cahn–Hilliard model if M is large. We will discuss it in more details next (see Fig. 5.6).

#### 5.2. Assessment of the numerical schemes on benchmark problems

To further assess the numerical schemes, we numerically solve the model equations using the schemes with respect to two benchmark problems. Firstly we simulate the phase transition of crystal growth in 2D. We use time step  $\Delta t = 1 \times 10^{-3}$  and  $256 \times 256$  meshes in space in 2D simulations. A solid crystallite with Hexagonal ordering in 2D is initially placed in the center of the domain, which is assigned an average density  $\overline{\phi}$ . The initial condition is given by

$$\phi_0(\mathbf{r}) = \overline{\phi} + \mathbf{w}(\mathbf{r})(\mathbf{A}\phi_{\mathbf{s}}(\mathbf{r})), \tag{5.2}$$

where

$$w(\mathbf{r}) = \begin{cases} (1 - (\frac{|\mathbf{r} - \mathbf{r_0}|}{\mathbf{d_0}})^2)^2 & \text{if } \frac{|\mathbf{r} - \mathbf{r_0}|}{\mathbf{d_0}} \le 1, \\ 0 & \text{otherwise.} \end{cases}$$
 (5.3)

$$\phi_{s}(\mathbf{r}) = \cos(\frac{\mathbf{q}}{\sqrt{3}}\mathbf{y})\cos(\mathbf{q}\mathbf{x}) - \frac{1}{2}\cos(\frac{2\mathbf{q}}{\sqrt{3}}\mathbf{y}),\tag{5.4}$$

 $\mathbf{r_0}$  is the center coordinate of the domain, and  $\mathbf{d_0}$  is  $\frac{1}{6}$  of the domain length in the x-direction. The domain is given by

 $\Omega=[0,\frac{2\pi}{q}a]\times[0,\frac{\sqrt{3}\pi}{q}b]$ , a=10 and b=12. The other values are  $\varepsilon=0.325,\overline{\phi}=\frac{\sqrt{\varepsilon}}{2},A=\frac{4}{5}(\overline{\phi}+\frac{\sqrt{15\varepsilon-36\overline{\phi}^2}}{3})$  and  $q=\frac{\sqrt{3}}{2}$ . Fig. 5.1 shows time evolution of the crystal growth process computed using AC-EQ, CH-EQ, AC-P-EQ and AC-L-EQ schemes, respectively. In Fig. 5.1-(a), the crystal growth simulated by the Allen-Cahn model cannot preserve the Hexagonal ordering, different from the results simulated by the Cahn-Hilliard model in Fig. 5.1-(b) and the nonlocal Allen-Cahn models in Fig. 5.1-(c) and (d). The time evolution of mass and free energy are shown in Fig. 5.2-(a) and (b) respectively. The results computed by the EQ and SAV schemes for the same model (Allen-Cahn model, Cahn-Hilliard model and nonlocal Allen-Cahn models) are identical. We do not see any differences between the results of the Allen-Cahn model with a penalizing potential and the Allen-Cahn model with a Lagrange multiplier either. The mass decays in the Allen-Cahn model to nearly zero in finite time. In contrast, the mass in the Cahn-Hilliard model and the Allen-Cahn models with nonlocal constraints is conserved in the simulations. Meantime, the free energies of the Cahn-Hilliard model and the nonlocal Allen-Cahn model with nonlocal constraints reaches the steady state faster than that of the Cahn-Hilliard model.

Secondly we simulate another case of polycrystalline growth involving the grain boundary effect, where the two initial crystallites with a hexagonal configuration oriented in different direction (or misorientation) are put in the domain. Grain boundaries appear when the two crystals meet during the growth, which yields some orientational mismatch. The initial condition is given by

$$\phi_0(\mathbf{r}) = \overline{\phi} + \mathbf{w}(\mathbf{x})(\mathbf{A}\phi_s(\mathbf{r})), \tag{5.5}$$

where

$$w(\mathbf{r}) = \begin{cases} (1 - (\frac{|\mathbf{r}_1|}{\mathbf{d_0}})^2)^2 & \text{if } \frac{|\mathbf{r}_1|}{\mathbf{d_0}} \le 1, \\ (1 - (\frac{|\mathbf{r}_2|}{\mathbf{d_0}})^2)^2 & \text{if } \frac{|\mathbf{r}_2|}{\mathbf{d_0}} \le 1, \\ 0 & \text{otherwise,} \end{cases}$$

$$(5.6)$$

 $\mathbf{r_1} = \sqrt{(x - \frac{1}{2}x_0)^2 + (y - \frac{1}{2}y_0)^2}$ ,  $\mathbf{r_2} = \sqrt{(x - \frac{3}{2}x_0)^2 + (y - \frac{3}{2}y_0)^2}$  and  $(x_0, y_0)$  is the center of the domain. The other parameters and the domain are the same as in the first example. By doing an affine transformation of the Cartesian coordinates (x, y) to produce a rotation  $\theta$  in the domain, the modified coordinates  $(x_\theta, y_\theta)$  can be used to generate the crystallites in different directions,

$$x_{\theta} = \cos(\theta)x - \sin(\theta)y,$$
  

$$y_{\theta} = \sin(\theta)x + \cos(\theta)y.$$
(5.7)

We put two crystallites in the domain, the first one is defined as Eq. (5.7) with  $\theta=0$ , the second is defined with  $\theta=\frac{\pi}{8}$ . Fig. 5.3 depicts the grain boundary effect during polycrystalline growth computed by AC-SAV, CH-SAV, AC-P-SAV and AC-L-SAV schemes, respectively. The snapshots of the phase transitions computed by the Cahn-Hilliard and the nonlocal

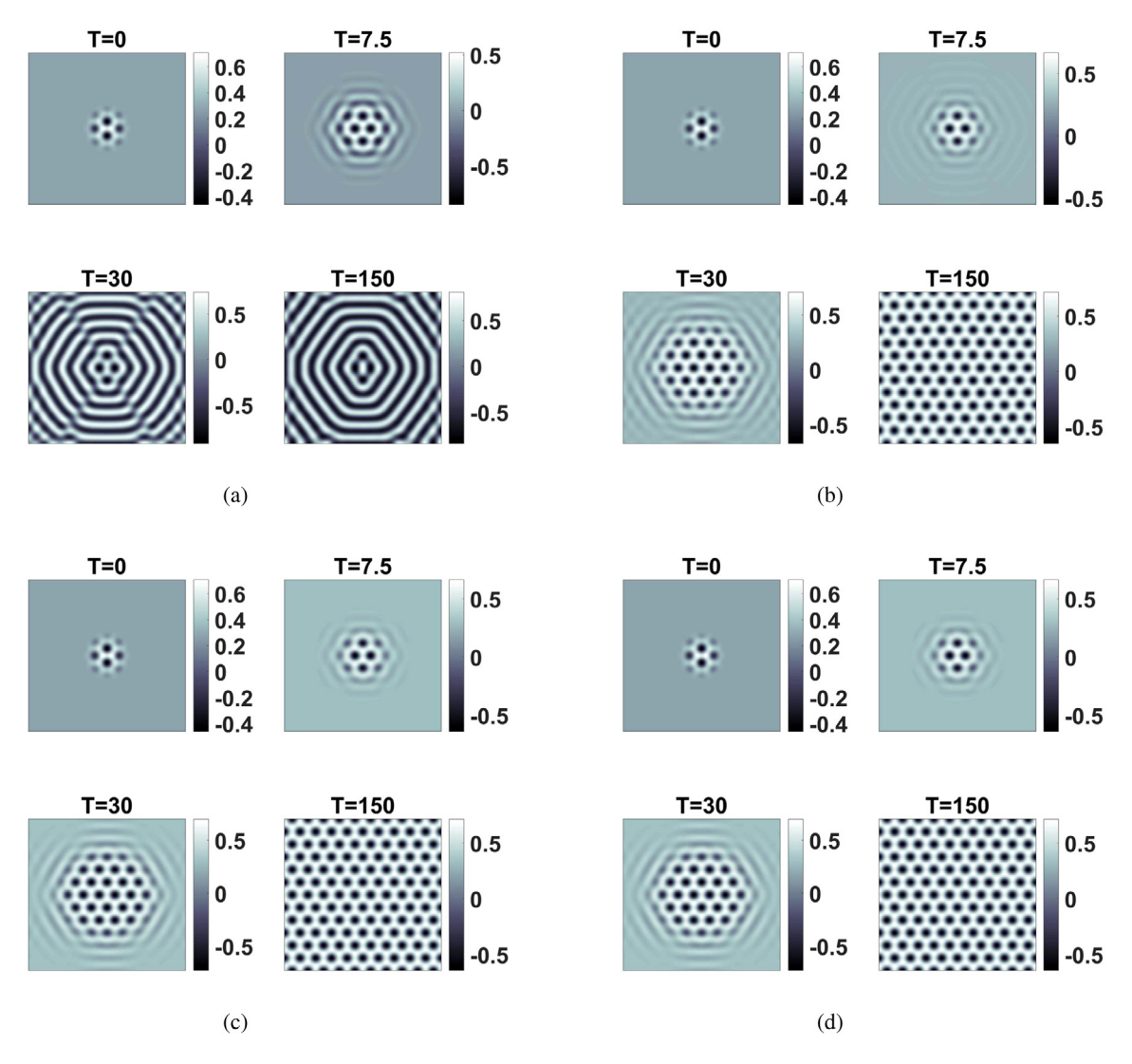


**Fig. 5.1.** Crystal growth simulated using the Allen–Cahn, Cahn–Hilliard and Allen–Cahn models with nonlocal constraints at M=1. (a)–(d) are computed using AC-EQ, CH-EQ, AC-P-EQ and AC-L-EQ schemes respectively. Snapshots of the atomistic density field  $\phi$  are depicted at T=0,7.5,30,150, respectively. Parameter  $\eta$  is set as  $1\times10^3$  in the AC-P-EQ/SAV schemes. We use time step  $\Delta t=1\times10^{-3}$  and  $256\times256$  space meshes in the 2D simulation. The Allen–Cahn model gives an erroneous result while the other models give comparable results.

Allen–Cahn models show the Hexagonal ordering are broken at the center at T=400. The time evolution of mass and free energy are shown in Fig. 5.4-(a) and (b), respectively. The mass in the Allen–Cahn model decays in time as expected. In contrast, the mass in the Cahn–Hilliard model and the nonlocal Allen–Cahn models are conserved during the simulation. Meanwhile, the free energies of the Cahn–Hilliard model and the nonlocal Allen–Cahn models are larger than that of the Allen–Cahn model. In Fig. 5.4-(b), the nonlocal Allen–Cahn models and the Cahn–Hilliard model predict comparable time evolution of the free energy but the nonlocal Allen–Cahn models reach the steady state first. The results computed by the EQ and SAV schemes for the same model (the Allen–Cahn model, Cahn–Hilliard model and nonlocal Allen–Cahn model) are nearly identical. We do not see any differences between the results of the Allen–Cahn model with a penalizing potential and the Allen–Cahn model with a Lagrange multiplier either.

To illustrate the time evolutionary behavior of the models, we conduct another simulation with three spatially isolated crystallites to begin with. Simulation results are shown in Fig. 5.5, where the free energy of the Allen–Cahn models with nonlocal constraints shows smaller value during the transient dynamical simulations shown.

We note that the results computed by the Allen–Cahn model with a penalizing potential and the Allen–Cahn model with a Lagrange multiplier in the above two examples at  $\eta=1\times 10^3$  are the same. However, the choice of  $\eta$  can certainly affect the outcome. In principle,  $\eta$  should be chosen as large as possible. However, when  $\eta$  is too large, the governing equation becomes very stiff, which forces one to use extremely small time-step size in order to resolve the

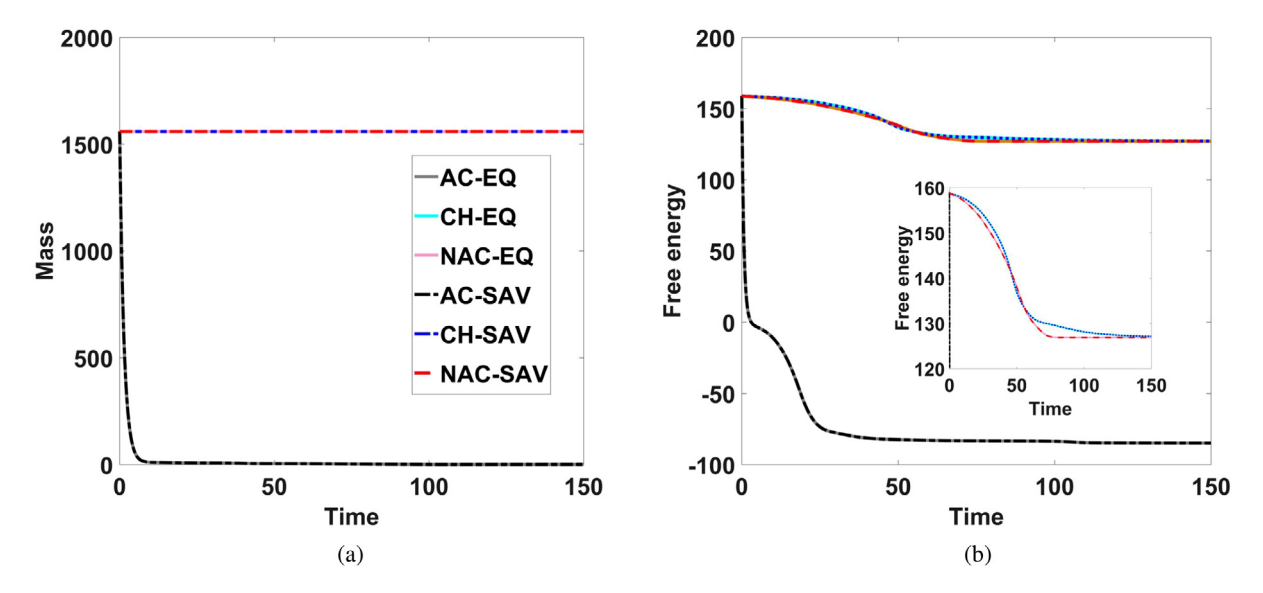


**Fig. 5.2.** Time evolution of the mass and free energy from the simulations for Allen–Cahn (AC), Cahn–Hilliard (CH) and nonlocal Allen–Cahn (NAC) models are shown in (a) and (b), respectively. Since the results computed by the Allen–Cahn model with nonlocal constraints are nearly identical, we only show time evolution of the mass and free energy computed using the AC-L-EQ scheme. We compare time evolution of the mass and free energy computed by the EQ and SAV schemes in (a) and (b). There is no difference between the results computed by the two methods. The mass computed using the Allen model vanishes before T = 10, whereas it is conserved in the Cahn–Hilliard and the Allen–Cahn model with nonlocal constraints. The free energy computed by all models are dissipative. The nonlocal Allen–Cahn models predict comparable free energy to the Cahn–Hilliard model but reach the steady state faster than the Cahn–Hilliard model does.

detail correctly. On the other hand, as we have shown in the two examples,  $\eta = 1 \times 10^3$  is good enough to produce the results that conserve mass very well.

Both Figs. 5.2 and 5.4 show that the free energy computed by the nonlocal Allen–Cahn models reach the steady state faster than that of the Cahn–Hilliard model, which is different from our previous results on a different free energy functional [58]. Especially, the simulations computed by the models with mobility coefficient M=1 and time steps  $1\times 10^{-2}$ ,  $1\times 10^{-4}$  show the afore-mentioned time evolution behavior. When the mobility is large, say M=10, and  $\Delta t=0.01$ , the CH-SAV produce an erroneous result while the others produce comparable ones. In practice, if the steady state is more important than the transient dynamics, one can enlarge the mobility coefficient of the models to accelerate the convergence to steady state. But, CH-SAV seems to have some accuracy issues with this approach at large time step sizes. The results of the nonlocal Allen–Cahn models in 5.6-(a) and (b) show better performance than the Cahn–Hilliard model does in Fig. 5.6-(c) and (d).

#### 6. Conclusions

We have developed a set of linear, second order, energy stable schemes for the Allen–Cahn model with nonlocal constraints that conserve mass and compared them with the energy stable, linear schemes for the Allen–Cahn and the Cahn–Hilliard model. These schemes are devised based on the energy quadratization strategy in the form of EQ and SAV formulation of original models, respectively. We show that they are unconditionally energy stable and uniquely solvable. All schemes can be solved using efficient numerical methods, making the models alternatives to the Cahn–Hilliard model to describe interface dynamics of immiscible materials while conserving mass. The nonlocal Allen–Cahn models show a faster coarsening rate than that of the Cahn–Hilliard model at the same mobility, but one can enlarge the mobility coefficient of the nonlocal Allen–Cahn model to accelerate their dynamics in case only steady states are of interest. In addition, we have compared the two Allen–Cahn models with nonlocal constraints numerically. The computational efficiency of the Allen–Cahn model with a penalizing potential is slightly better than the one with a Lagrange multiplier, but the accuracy of the former depends on a suitable choice of model parameter  $\eta$ . If the steady state is desired rather than the transient dynamical behavior, large time step size and mobility coefficient can be used to accelerate the simulation. In the end, we show that the nonlocal Allen–Cahn models perform better that the Cahn–Hilliard model in the case of a large time step and mobility coefficient.

#### Acknowledgments

The research is partially supported by NSFC awards #11571032, #91630207 and NSAF-U1530401.

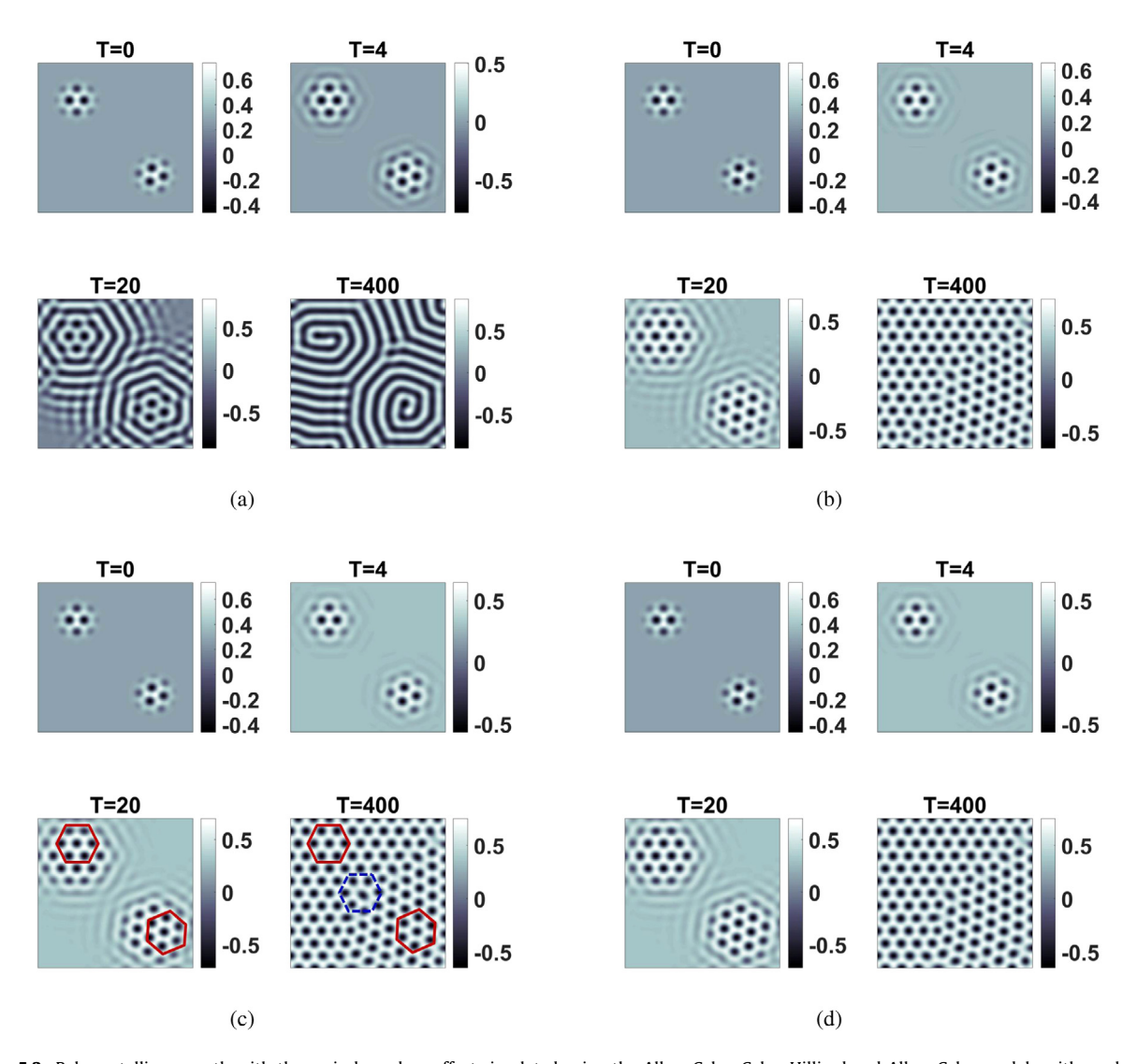


**Fig. 5.3.** Polycrystalline growth with the grain boundary effect simulated using the Allen–Cahn, Cahn–Hilliard and Allen–Cahn models with nonlocal constraints at M=1. (a)–(d) are computed using AC-SAV, CH-SAV, AC-P-SAV and AC-L-SAV scheme, respectively. Snapshots of the atomistic density field  $\phi$  are taken at T=0, 4, 20, 400, respectively. Different growth patterns start affecting each other at T=0 and the hexagonal ordering breaks down eventually at the interface of the polycrystalline. The solid hexagonal ordering and dash non-hexagonal ordering are shown in (c). Parameter  $\eta$  is set as  $1\times 10^3$ . We use time step  $\Delta t=1\times 10^{-3}$  and  $256\times 256$  space meshes in the 2D simulation.

#### Appendix. Shermann-Morrison formula and its application to solving integro-differential equations

Here we give a brief review over the Sherman–Morrison formula [59] and explain its applications in the practical implementation of our various relevant schemes.

Suppose A is an invertible square matrix, and u, v are column vectors. Then  $A + uv^T$  is invertible iff  $1 + v^T A^{-1} u \neq 0$ . If  $A + uv^T$  is invertible, then its inverse is given by

$$(A + uv^{T})^{-1} = A^{-1} - \frac{A^{-1}uv^{T}A^{-1}}{1 + v^{T}A^{-1}u}.$$
(A.1)

So if Ay = b and Az = u,  $(A + uv^T)x = b$  has the solution given by

$$x = y - \frac{v^T y}{1 + v^T z} z. \tag{A.2}$$

For the integral term(s) in the semi-discrete schemes in this study such as (4.58), we need to discretize it properly.  $\forall f$ , we discretize  $\int_{\mathcal{Q}} f d\mathbf{r}$  using the composite trapezoidal rule and adding all the elements of the new matrix  $w_1 w_2^T f$ , where

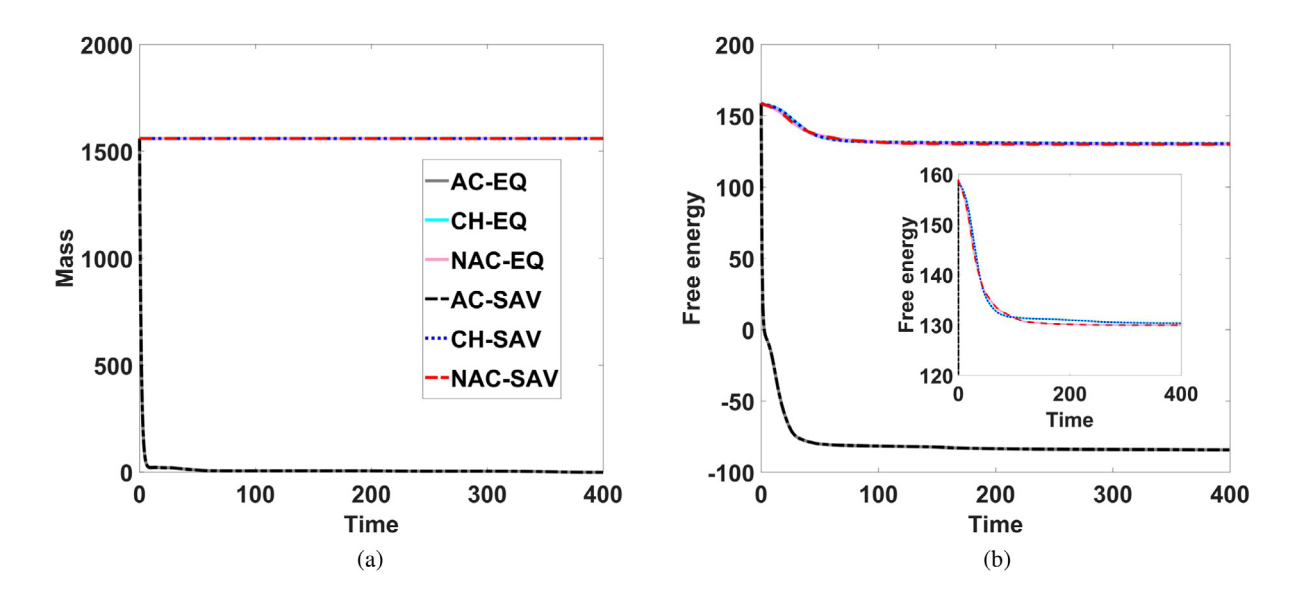
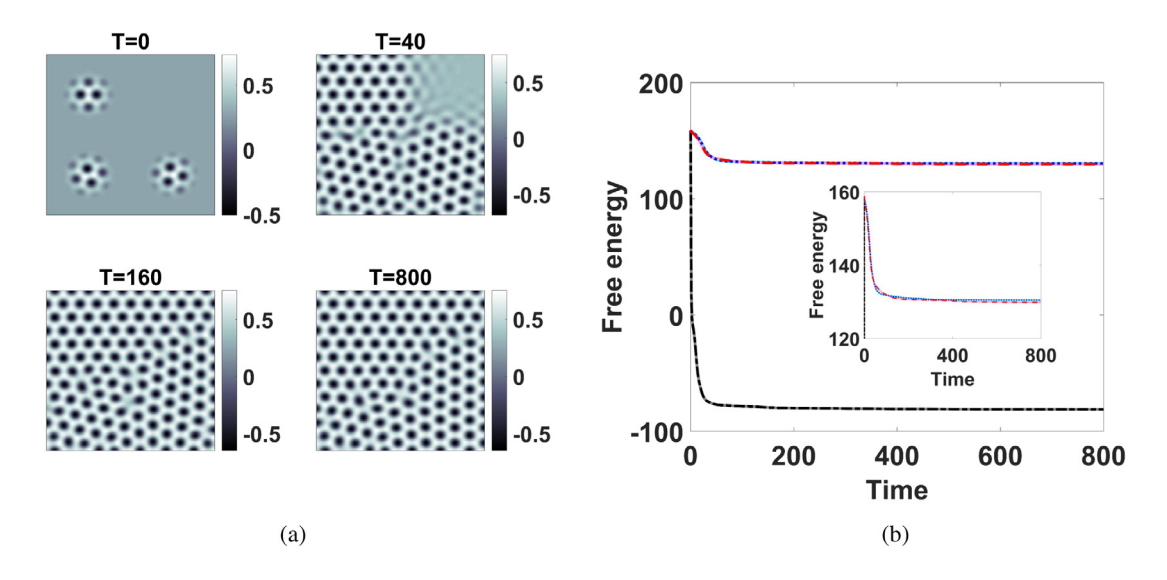
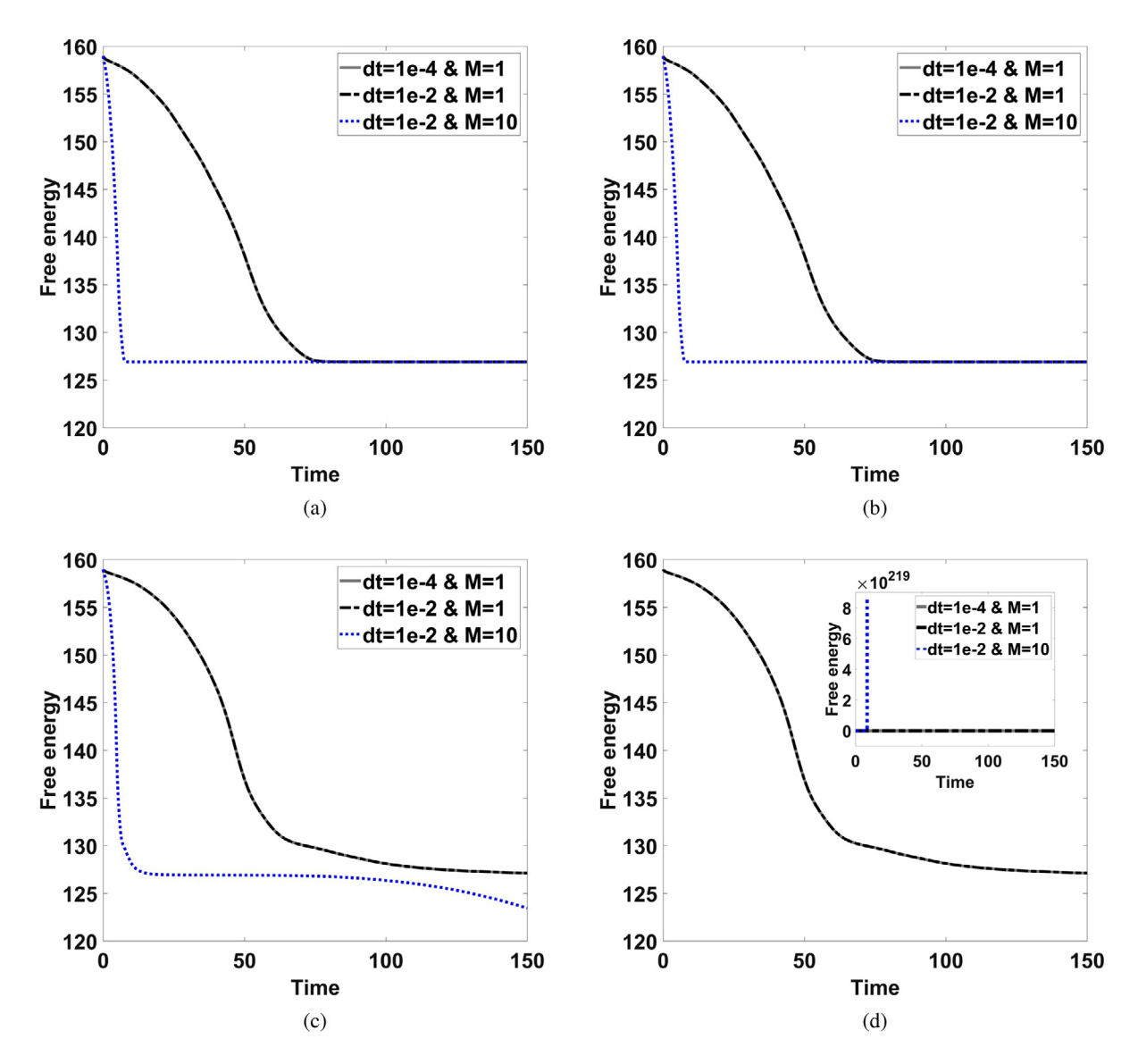


Fig. 5.4. Time evolution of mass and free energy from the simulation for Allen-Cahn (AC), Cahn-Hilliard (CH) and nonlocal Allen-Cahn (NAC) models are shown in (a) and (b), respectively. Since the dynamical behavior of the Allen-Cahn model with nonlocal constraints are the same, we only show the time evolution of mass and free energy computed using the AC-L-EQ scheme. We compare the time evolution of mass and free energy computed by the EQ and SAV schemes in (a) and (b). We do not see any differences between the results computed by the EQ and SAV methods. The mass computed using the Allen-Cahn model vanishes before T=50, whereas it is conserved by the Cahn-Hilliard and the Allen-Cahn model with nonlocal constraints. Free energy computed by all models are dissipative. Similarly, the nonlocal Allen-Cahn and Cahn-Hilliard model predict comparable results in the free energy, but the free energy in the nonlocal models reach the steady state faster than the Cahn-Hilliard model does.



**Fig. 5.5.** Polycrystalline growth with the grain boundary effect simulated using the Allen–Cahn, Cahn–Hilliard and Allen–Cahn models with nonlocal constraints at M=1. (a) Results computed using AC-L-SAV scheme, in which snapshots of the atomistic density field  $\phi$  are shown at T=0, 40, 160, 800, respectively. Different growth patterns start affecting each other soon after start up and the hexagonal ordering breaks down at the interface of the polycrystalline forming grain boundaries. Parameter  $\eta$  is set as  $1 \times 10^3$ . We use time step  $\Delta t = 1 \times 10^{-3}$  and  $256 \times 256$  space meshes in the 2D simulation. (b). The free energy function of the four models as a function of time. The free energy of the Allen–Cahn model with a Lagrange multiplier yields the smaller free energy during the transient dynamical simulations among the four models.

 $w_1 = \frac{h_x}{2}S$ ,  $w_2 = \frac{h_y}{2}S$ ,  $h_x$ ,  $h_y$  are the spatial step sizes and  $S = [1, 2, 2, ..., 2, 2, 1]^T$ . For convenience, we use  $w_1w_2^Tf$  to represent the integral discretized by the composite trapezoidal rule.



**Fig. 5.6.** Comparison among the nonlocal Allen–Cahn models and the Cahn–Hilliard model with large time step size and large mobility coefficients. (a)–(d) are simulated by AC-L-EQ, AC-L-SAV, CH-EQ, CH-SAVscheme with  $\Delta t = 1 \times 10^{-4}$ , M = 1,  $\Delta t = 1 \times 10^{-2}$ , M = 1 and  $\Delta t = 1 \times 10^{-2}$ , M = 10, respectively. The results show that the nonlocal Allen–Cahn model with a large time step size and large mobility coefficient (a) and (b) performs better than that of the Cahn–Hilliard model (c) and (d). The initial conditions and other parameters are chosen the same as those in Fig. 5.1.

To solve equation (4.58), we discretize the integral or the inner product of functions  $(c, \phi^{n+1})d$  as  $uv^T\phi^{n+1}$ . The scheme is recast to  $A\phi^{n+1} + uv^T\phi^{n+1} = b^n$ . After using the Sherman–Morrison formula, we get

$$\phi^{n+1} = A^{-1}b^n - \frac{v^T A^{-1}b^n}{1 + v^T A^{-1}u}A^{-1}u, \tag{A.3}$$

In the inner product of vectors, (4.58) can be rewritten into

$$\phi^{n+1} = A^{-1}b^n - \frac{\langle c, A^{-1}b^n \rangle}{1 + \langle c, A^{-1}d \rangle} A^{-1}d. \tag{A.4}$$

So, indeed the approach we take in the study using the discrete inner product is essentially equivalent to applying the Sherman–Morrison formula.

#### References

- [1] K.R. Elder, Mark Katakowski, Mikko Haataja, Martin Grant, Modeling elasticity in crystal growth, Phys. Rev. Lett. 88 (24) (2002) 245701.
- [2] K.R. Elder, Martin Grant, Modeling elastic and plastic deformations in nonequilibrium processing using phase field crystals, Phys. Rev. E 70 (5) (2004) 051605
- [3] Nikolas Provatas, Ken Elder, Phase-Field Methods in Materials Science and Engineering, John Wiley & Sons, 2011.
- [4] A. Jaatinen, T. Ala-Nissila, Extended phase diagram of the three-dimensional phase field crystal model, J. Phys.: Condens. Matter 22 (20) (2010) 205402.
- [5] Alain Karma, Wouter-Jan Rappel, Phase-field method for computationally efficient modeling of solidification with arbitrary interface kinetics, Phys. Rev. E 53 (4) (1996) R3017.
- [6] K.R. Elder, Nikolas Provatas, Joel Berry, Peter Stefanovic, Martin Grant, Phase-field crystal modeling and classical density functional theory of freezing, Phys. Rev. B 75 (6) (2007) 064107.
- [7] N. Provatas, J.A. Dantzig, B. Athreya, P. Chan, P. Stefanovic, N. Goldenfeld, K.R. Elder, Using the phase-field crystal method in the multi-scale modeling of microstructure evolution, Jom 59 (7) (2007) 83–90.
- [8] Ebrahim Asadi, Mohsen Asle Zaeem, A review of quantitative phase-field crystal modeling of solid-liquid structures, Jom 67 (1) (2015) 186–201.
- [9] Rainer Backofen, Andreas Rätz, Axel Voigt, Nucleation and growth by a phase field crystal (pfc) model, Phil. Mag. Lett. 87 (11) (2007) 813-820.
- [10] Rainer Backofen, Axel Voigt, A phase-field-crystal approach to critical nuclei, J. Phys.: Condens. Matter 22 (36) (2010) 364104.
- [11] Gyula I. Tóth, György Tegze, Tamás Pusztai, Gergely Tóth, László Gránásy, Polymorphism, crystal nucleation and growth in the phase-field crystal model in 2d and 3d, J. Phys.: Condens. Matter 22 (36) (2010) 364101.
- [12] Nicholas Guttenberg, Nigel Goldenfeld, Jonathan Dantzig, Emergence of foams from the breakdown of the phase field crystal model, Phys. Rev. E 81 (6) (2010) 065301.
- [13] Joel Berry, K.R. Elder, Martin Grant, Simulation of an atomistic dynamic field theory for monatomic liquids: Freezing and glass formation, Phys. Rev. E 77 (6) (2008) 061506.
- [14] Hartmut Löwen, A phase-field-crystal model for liquid crystals, J. Phys.: Condens. Matter 22 (36) (2010) 364105.
- [15] N. Pisutha-Arnond, V.W.L. Chan, K.R. Elder, K. Thornton, Calculations of isothermal elastic constants in the phase-field crystal model, Phys. Rev. B 87 (1) (2013) 014103.
- [16] Jesper Mellenthin, Alain Karma, Mathis Plapp, Phase-field crystal study of grain-boundary premelting, Phys. Rev. B 78 (18) (2008) 184110.
- [17] Xiaofeng Yang, James J. Feng, Chun Liu, Jie Shen, Numerical simulations of jet pinching-off and drop formation using an energetic variational phase-field method, J. Comput. Phys. 218 (1) (2006) 417–428.
- [18] Jacob Rubinstein, Peter Sternberg, Nonlocal reaction diffusion equations and nucleation, IMA J. Appl. Math. 48 (3) (1992) 249-264.
- [19] Hongwei Li, Lili Ju, Chenfei Zhang, Qiujin Peng, Unconditionally energy stable linear schemes for the diffuse interface model with peng–robinson equation of state, J. Sci. Comput. 75 (2) (2018) 993–1015.
- [20] Qiang Du, Chun Liu, Xiaoqiang Wang, A phase field approach in the numerical study of the elastic bending energy for vesicle membranes, J. Comput. Phys. 198 (2) (2004) 450–468.
- [21] Charles M. Elliott, A.M. Stuart, The global dynamics of discrete semilinear parabolic equations, SIAM J. Numer. Anal. 30 (6) (1993) 1622-1663.
- [22] Xiaolin Fan, Jisheng Kou, Zhonghua Qiao, Shuyu Sun, A componentwise convex splitting scheme for diffuse interface models with van der waals and peng-robinson equations of state, SIAM J. Sci. Comput. 39 (1) (2017) B1–B28.
- [23] David J. Eyre, Unconditionally gradient stable time marching the Cahn-Hilliard equation, MRS Online Proceedings Library Archive, 529, 1998.
- [24] Steven M. Wise, Cheng Wang, John S. Lowengrub, An energy-stable and convergent finite-difference scheme for the phase field crystal equation, SIAM J. Numer. Anal. 47 (3) (2009) 2269–2288.
- [25] Jie Shen, Cheng Wang, Xiaoming Wang, Steven M. Wise, Second-order convex splitting schemes for gradient flows with ehrlich-schwoebel type energy: application to thin film epitaxy, SIAM J. Numer. Anal. 50 (1) (2012) 105–125.
- [26] Cheng Wang, Xiaoming Wang, Steven M. Wise, Unconditionally stable schemes for equations of thin film epitaxy, Discrete Contin. Dyn. Syst. 28 (1) (2010) 405–423.
- [27] Daozhi Han, Xiaoming Wang, A second order in time, uniquely solvable, unconditionally stable numerical scheme for cahn-hilliard-navier-stokes equation, J. Comput. Phys. 290 (2015) 139–156.
- [28] Jie Shen, Xiaofeng Yang, Numerical approximations of allen-cahn and cahn-hilliard equations, Discrete Contin. Dyn. Syst. 28 (4) (2010) 1669–1691.
- [29] Qiang Du, Lili Ju, Xiao Li, Zhonghua Qiao, Stabilized linear semi-implicit schemes for the nonlocal cahn-hilliard equation, J. Comput. Phys. 363 (2018) 39–54.
- [30] Wenbin Chen, Daozhi Han, Xiaoming Wang, Uniquely solvable and energy stable decoupled numerical schemes for the cahn-hilliard-stokes-darcy system for two-phase flows in karstic geometry, Numer. Math. 137 (1) (2017) 229–255.
- [31] Jia Zhao, Xiaofeng Yang, Yuezheng Gong, Xueping Zhao, Xiaogang Yang, Jun Li, Qi Wang, A general strategy for numerical approximations of non-equilibrium models-part i: thermodynamical systems, Int. J. Numer. Anal. Model. 15 (6) (2018) 884–918.
- [32] Xiaofeng Yang, Jia Zhao, Qi Wang, Numerical approximations for the molecular beam epitaxial growth model based on the invariant energy quadratization method, J. Comput. Phys. 333 (2017) 104–127.
- [33] Yuezheng Gong, Jia Zhao, Xiaogang Yang, Qi Wang, Fully discrete second-order linear schemes for hydrodynamic phase field models of binary viscous fluid flows with variable densities, SIAM J. Sci. Comput. 40 (1) (2018) B138–B167.
- [34] Yuezheng Gong, Jia Zhao, Qi Wang, Linear second order in time energy stable schemes for hydrodynamic models of binary mixtures based on a spatially pseudospectral approximation, Adv. Comput. Math. (2018) 1–28.
- [35] Jie Shen, Jie Xu, Jiang Yang, The scalar auxiliary variable (sav) approach for gradient flows, J. Comput. Phys. 353 (2018) 407-416.
- [36] Suchuan Dong, Zhiguo Yang, Lianlei Lin, A Family of Second-Order Energy-Stable Schemes for Cahn-Hilliard Type Equations, arXiv preprint arXiv:1803.06047, 2018.
- [37] Lin Wang, Haijun Yu, On efficient second order stabilized semi-implicit schemes for the cahn-hilliard phase-field equation, J. Sci. Comput. (2017) 1–25.
- [38] Yuezheng Gong, Qi Wang, Jia Zhao, Aritrary high order unconditionally energy stable schemes for gradient flow models, SIAM J. Sci. Comput. (2019).
- [39] Xiaofeng Yang, Lili Ju, Linear and unconditionally energy stable schemes for the binary fluid csurfactant phase field model, Comput. Methods Appl. Mech. Engrg. 318 (2017) 1005–1029.
- [40] Jia Zhao, Qi Wang, Xiaofeng Yang, Numerical approximations to a new phase field model for two phase flows of complex fluids, Comput. Methods Appl. Mech. Engrg. 310 (2016) 77–97.
- [41] Jia Zhao, Qi Wang, Xiaofeng Yang, Numerical approximations for a phase field dendritic crystal growth model based on the invariant energy quadratization approach, Internat. J. Numer. Methods Engrg. 110 (3) (2017).

- [42] Lizhen Chen, Jia Zhao, Xiaofeng Yang, Regularized linear schemes for the molecular beam epitaxy model with slope selection, Appl. Numer. Math. 128 (2018) 139–156.
- [43] Xiaofeng Yang, Efficient schemes with unconditionally energy stability for the anisotropic Cahn-Hilliard Equation using the stabilized-Scalar Augmented Variable (S-SAV) approach, arXiv preprint arXiv:1804.02619, 2018.
- [44] Jia Zhao, Xiaofeng Yang, Jun Li, Qi Wang, Energy stable numerical schemes for a hydrodynamic model of nematic liquid crystals, SIAM J. Sci. Comput. 38 (5) (2016) A3264–A3290.
- [45] Jia Zhao, Xiaofeng Yang, Yuezheng Gong, Qi Wang, A novel linear second order unconditionally energy stable scheme for a hydrodynamic-tensor model of liquid crystals, Comput. Methods Appl. Mech. Engrg. 318 (2017) 803–825.
- [46] Jia Zhao, Xiaofeng Yang, Jie Shen, Qi Wang, A decoupled energy stable scheme for a hydrodynamic phase-field model of mixtures of nematic liquid crystals and viscous fluids, J. Comput. Phys. 305 (2016) 539–556.
- [47] Lars Onsager, Reciprocal relations in irreversible processes. i., Phys. Rev. 37 (4) (1931) 405.
- [48] Lars Onsager, Reciprocal relations in irreversible processes. ii., Phys. Rev. 38 (12) (1931) 2265.
- [49] C. Wang, Steven M. Wise, An energy stable and convergent finite-difference scheme for the modified phase field crystal equation, SIAM J. Numer. Anal. 49 (3) (2011) 945–969.
- [50] Jie Shen, Jie Xu, Convergence and error analysis for the scalar auxiliary variable (sav) schemes to gradient flows, SIAM J. Numer. Anal. 56 (5) (2018) 2895–2912.
- [51] Xiaofeng Yang, Daozhi Han, Linearly first-and second-order, unconditionally energy stable schemes for the phase field crystal model, J. Comput. Phys. 330 (2017) 1116–1134.
- [52] Zhengzheng Hu, Steven M. Wise, Cheng Wang, John S. Lowengrub, Stable and efficient finite-difference nonlinear-multigrid schemes for the phase field crystal equation, J. Comput. Phys. 228 (15) (2009) 5323–5339.
- [53] Matt Elsey, Benedikt Wirth, A simple and efficient scheme for phase field crystal simulation?, ESAIM Math. Model. Numer. Anal. 47 (5) (2013) 1413–1432.
- [54] Hector Gomez, Xesús Nogueira, An unconditionally energy-stable method for the phase field crystal equation, Comput. Methods Appl. Mech. Engrg. 249 (2012) 52-61.
- [55] Hector Gomez, Thomas J.R. Hughes, Provably unconditionally stable, second-order time-accurate, mixed variational methods for phase-field models, J. Comput. Phys. 230 (13) (2011) 5310–5327.
- [56] György Tegze, Gurvinder Bansel, Gyula I Tóth, Tamás Pusztai, Zhongyun Fan, László Gránásy, Advanced operator splitting-based semi-implicit spectral method to solve the binary phase-field crystal equations with variable coefficients, J. Comput. Phys. 228 (5) (2009) 1612–1623.
- [57] Philippe Vignal, Lisandro Dalcin, Donald L. Brown, Nathan Collier, Victor M. Calo, An energy-stable convex splitting for the phase-field crystal equation, Comput. Struct. 158 (2015) 355–368.
- [58] Xiaobo Jing, Jun Li, Xueping Zhao, Qi Wang, Second order linear energy stable schemes for allen-cahn equations with nonlocal constraints, arXiv preprint arXiv:1810.05311, 2018.
- [59] E. Bodewig, Matrix Calculus, North, p17, Holland Publishing Co., Amsterdam, 1959.